International Journal of Pharmaceutics 650 (2024) 123704

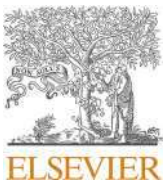

Contents lists available at ScienceDirect

International Journal of Pharmaceutics

journal homepage: www.elsevier.com/locate/ijpharm

Engineering a novel water-in-oil biocompatible microemulsion system for the ocular delivery of dexamethasone sodium phosphate in the treatment of acute uveitis

Dina M. Abd-elaty, Rania A.H. Ishak *, Rihab Osman, Ahmed S. Geneidi

Department of Pharmaceutics and Industrial Pharmacy, Faculty of Pharmacy, Ain Shams University, 11566 Cairo, Egypt

ARTICLE INFO

Keywords:
Biocompatible
Microemulsion
Uveitis
Dexamethasone sodium phosphate
Ocular delivery

ABSTRACT

Due to their unique characteristics, microemulsions (ME) represent one of the most promising delivery systems which can conquer poor ocular drug bioavailability providing long residence time. Development of a ME system, relying on the use of a safe and non-irritant surfactant combination derived from sustainable resources and which can consolidate the small ME droplets, is the goal of this work. Herein, we report the design and characterization of a novel biocompatible, eco-friendly ME system loaded with the hydrophilic dexamethasone sodium phosphate (DEXP) using a novel surfactant mixture composed of D-α-tocopherol polyethylene glycol succinate (TPGS) and Plantacare® (coco-Glycosides). Capryol™ PGMC and double-distilled water were used as the respective oil and aqueous phases and the MEs were prepared by the water titration method, suitable for scaling up. Optimization of ME formulae was conducted by varying Plantacare® grades, TPGS to Plantacare® mass ratios and drug loading. The formulae were characterized in terms of physical appearance, droplet size (PS), size distribution (PDI), zeta potential (ZP), and stability. The optimized DEXP-loaded ME formula attained acceptable PS, PDI, and ZP values of 43 ± 5 nm, 0.35 ± 0.07, −12 ± 4 mV, respectively. TEM images confirmed a small PS ≤ 100 nm. The *in vivo* safety of ME was proved by the Draize test. The ME formula prompted excellent mucoadhesion and transcorneal permeation. The confocal studies showed deep penetration into the rabbits' corneas. *In vivo* studies using endotoxin-induced uveitis showed high ocular efficacy and a significant reduction in inflammatory cells, including interleukin-6 (IL-6) and tumor necrosis factor-α (TNF-α). The obtained results elect the novel engineered ME system as a promising tool for the ocular delivery of hydrophilic moieties in the management of various ophthalmic diseases.

1. Introduction

Uveitis is an emerging type of acute inflammation that affects the ciliary body, the iris, and the choroid composing the uvea. It can extend to the retina, vitreous, sclera and optic nerve. Patients suffering from uveitis usually experience pain in the eye, redness of the conjunctiva, and photophobia. If left without treatment, acute or chronic inflammation of the eye can result in temporary or permanent vision loss through the formation of eye cataracts, complete optic nerve damage, permanent destruction of the blood-aqueous barrier, the formation of

Abbreviations: APE, alkylphenol ethoxylate, APGs, alkyl polyglycosides; CLSM, confocal laser scanning microscopy; co-SAA, Co-surfactant; CPP, critical packing parameter; D, diffusion coefficient; DEX, dexamethasone; DEXP, dexamethasone sodium phosphate; DLS, dynamic light scattering; DSC, Differential scanning calorimetery; EIU, Endotoxin Induced Uveitis model; ER, enhancement ratio; h, hour; FT-IR, Fourier Transform Infrared Spectroscopy; Ho, spontaneous curvature; H&E, hematoxylin and eosin; HCl, hydrochloric acid; HLB, hydrophile lipophile balance; HPLC, high performance liquid chromatography; HRP, horseradish Peroxidase; HR-TEM, High resolution-transmission electron microscope; γw/o, interfacial tension; IL-6, Interleukin-6; IOP, intraocular pressure; Jss, drug transcorneal flux; KBr, potassium bromide; LDA, laser Doppler anemometry; LPS, lipopolysaccharide, M, molar; ME, Microemulsion; min, minutes; NaOH, sodium hydroxide; o/w, oil in water; OD, optical density; P, statistical significance level; Papp, apparent permeability coefficient; PBS, phosphate buffer saline; PDI, Poly dispersity index; PEG, polyethylene glycol; PS, Particle size; Q, cumulative amount of drug released per unit surface area at time t; REC, record; RI, refractive index; S mix, surfactant/co-surfactant mixture; SAAs, surfactants; SD, standard deviation; SMEDDS, Self-Microemulsifying Drug Delivery System; t, time; T, transmittance; T-test, student, s test; TNF-α, tumor necrosis factor-α; TPGS, D-α-tocopherol polyethylene glycol succinate; UV, ultra violet; w/o, water in oil; λ max, lambda max; ZP, Zeta potential.

* Corresponding author.
E-mail address: raniaaziz@pharma.asu.edu.eg (R.A.H. Ishak).

https://doi.org/10.1016/j.ijpharm.2023.123704
Received 12 October 2023; Received in revised form 4 December 2023; Accepted 11 December 2023
Available online 12 December 2023

synechiae, inflammation of the vitreous and cystoid macular swelling. Uveitis has been involved in nearly 10 % of all the blindness cases in the world (Zou et al., 2019).

The conventional treatment of anterior uveitis relies on the use of topical corticosteroids, which reduce inflammation. Patients treated with corticosteroids are regularly evaluated, with an organized corticosteroid lowering protocol monitored by the clinical condition of the patient. Dexamethasone sodium phosphate (DEXP) is a water-soluble salt of the basic corticosteroid moiety, DEX. It suffers from poor penetration through the ocular tissues with rapid metabolism in these tissues and clearance by tears, requiring frequent administration (Yin et al., 2023). DEXP has been used in the management of a large variety of ocular inflammatory problems such as keratitis, iritis, blepharitis, uveitis, conjunctivitis, macular edema, and post-operative eye surgery in the form of eye drops, eye ointment, oral tablets, intravitreal injections, and intraocular implants. The efficacy of corticosteroid eye drops is usually limited by their relatively low ocular bioavailability and consequent multiple dosing. Chronic treatment for a long period of time can lead to undesirable side effects like elevation of the intraocular pressure (IOP) and the development of eye cataract **(Cohen et al., 2012)**. Eye ointments impart a greasy feeling (Agarwal & Rupenthal, 2023); oral tablets lead to high drug systemic concentration with possible toxicity; while intravitreal injections and intraocular implants require invasive administration (Rajput et al., 2022).

Microemulsions (MEs) are colloidal dispersions stabilized by a surfactant (SAA) and a co-surfactant (co-SAA), and the size of the dispersed domains is typically less than 100 nm (Ugurl, 2023). Ocular MEs have been successfully used to solubilize drugs with different polarities and achieve a sustained drug release with a high drug concentration by increasing drug penetration into the deep structures of the eye due to their magnificent properties and small droplet size (Akbari et al., 2023; Al-mahallawi et al., 2021; Billowria et al., 2023; Cardoso et al., 2022; **2023;** Dutta et al., 2023; Palaria et al., 2023). This will eventually decrease the number of drug administrations, lower the side effects, achieve higher patient compliance, and elevate the ocular bioavailability, thus superseding conventional ocular preparations. Water-in-oil (w/o) MEs are used for the delivery of hydrophilic drugs in order to increase the viscosity of the formula and consequently increase the retention within the eye (Elmotasem & Awad, 2020).

However, conventional MEs usually contain a large proportion of surfactants, which may provoke toxicity in the ocular tissues. This necessitates the development of a biocompatible ME system to increase drug permeation and bioavailability without causing any ocular toxicity (Bernal-Jácome et al., 2023). Talking about progress in surfactants, several types have been established, including zero-sulfate surfactants, alkylphenol ethoxylate (APE)-free products, phosphate-free detergent products, and surfactants derived from natural sources. Alkyl polyglycosides (APGs) are a new class of sugar-based, non-ionic surfactants derived from starch and oils from plant sources. Plant oils play a critical role as renewable resources due to their wide existence and unique versatility (Jain et al., 2023). Compared to conventional SAA, APGs exhibit higher dermal and ocular safety, better biodegradability, and special foam properties, in addition to their potential cleaning and wetting properties, which promote their use in ocular preparations (Kaur et al., 2022).

D-α-tocopherol polyethylene glycol succinate (TPGS) is a non-ionic surfactant produced by the esterification of vitamin E with a polyethylene glycol (PEG-1000) moiety. TPGS has an HLB value of 13.2 and has been used as a solubilizer, an emulsifier, and a wetting agent. It also has a significant antioxidant property, which potentiates its role in many different ocular preparations to resolve the oxidative stress accompanied by many ocular problems such as increase in the IOP, cataract, and degenerative macular disease (Ali et al., 2023). Capryol™ PGMC is a hydrophobic oil, propylene glycol mono- and dicaprylate (type I) NF, consisting of mono and di-esters of propylene glycol of caprylic acid (C8). It can be considered a non-ionic, water-insoluble Co-SAA used in oral lipid-based formulae, self-microemulsifying drug delivery systems (SMEDDS), and self-emulsifying drug delivery systems (SEDDS), as well as a solubilizer in topical dosage forms (Hanaa et al., 2013).

The aim of this work was to establish a novel w/o ME system relying on the use of biocompatible components originating from sustainable resources, *viz.*, the novel surfactant combination composed of Plantacare® 818-UP (Coco-Glycoside), a sugar-based surfactant from the APGs class, and TPGS without the inclusion of any *co*-surfactant. DEXP was incorporated as a model hydrophilic anti-inflammatory drug, and the ME was fully characterized and then evaluated for safety using the Draize test and for efficacy using an endotoxin-induced uveitis animal model. The levels of various inflammatory messengers such as tumor necrosis factor- (TNF-α) and interleukin-6 (IL-6) as well as significant clinical manifestations and histopathological changes within the ocular tissues were tracked and measured (Zhang & Zhang, 2023) to evaluate the efficacy of the prepared ME formulation relative to the market product.

2. Materials and methods

2.1. Materials

Dexamethasone sodium phosphate (DEXP) was kindly supplied by Egyptian International Pharmaceutical Industries Co. (E.I.P.I.CO), Egypt. Plantacare® 818-UP (coco-glucoside, a C8-C16 fatty alcohol glycoside) and Plantacare® 1200 UP (lauryl glucoside, D-Glucopyranose, oligomeric, C10-C16-alkyl glycoside) were generously provided by BASF Co., Germany. D-α-tocopherol polyethylene glycol succinate (TPGS) was kindly provided by Isochem, France. Caproyl™ PGMC (propylene glycol mono- and dicaprylate Type I NF) was kindly provided by Gattefossé, France. Diethyl ether was purchased from Alpha Chemicals, India. Ethyl alcohol, absolute ethanol, acetonitrile (HPLC grade), and Rhodamine-b were supplied from Fischer Co., London, UK. Disodium hydrogen mono-ortho phosphate, Amaranth, mono-sodium dihydrogen phosphate, hydrochloric acid (HCl), sodium hydroxide (NaOH), sodium chloride (NaCl), acetone, paraformaldehyde, phosphoric acid, potassium bromide (KBr) pellets, isotonic saline, formol saline, xylene, propyl paraben, hematoxylin and eosin (H&E) were bought from Adwic, El-Nasr Pharmaceutical Co. Cairo, Egypt. Sabouraud dextrose agar was provided from Quest Park company, Heywood, UK. Thioglycolate broth was supplied from Oxoid LTD, Basingstoke, UK. Double-distilled water was provided from GFL Water Distillator, Germany. Escherichia coli 0111-B4 lipopolysaccharide (LPS) was purchased from Sigma Aldrich Chemical Co., St. Louis, USA. Interleukin-6 (Il-6); tumor necrosis factor-α (TNF-α) and rat assay kits; specific antibody Avidin-Horseradish Peroxidase (HRP); biotinylated detection antibody were bought from Bio-Rad Laboratories, CA, USA. New Zealand rabbits (2–3 kg) and male albino Wistar rats of 8 weeks old, each weighing approximately 180 g, were supplied from the animal house at the Faculty of Pharmacy, Ain Shams University. Freshly excised bovine corneas were supplied from a local slaughterhouse.

2.2. Methods

2.2.1. Preparation of TPGS/Plantacare®-based MEs

The MEs were prepared from the oil (Capryol™ PGMC), different ratios of the surfactant mixture (Smix), TPGS and Plantacare®, and double-distilled water using the aqueous titration method. The pseudo-ternary phase diagrams were then constructed with the aid of TriDraw® software (CHEMIX software, Version 2.9, Arne Standenes, Norway) for identifying the ME regions. MEs with varying compositions were selected from the region representing the one-phase system, characterized in terms of internal phase droplets' particle size, size distribution, and surface charge, and then subjected to stability studies. The effects of the following factors were evaluated:

2.2.1.1. Effect of Plantacare® type. Two different grades of Plantacare® were tried, *viz.* Plantacare® 818-UP and Plantacare® 1200.

2.2.1.2. Effect of TPGS to Plantacare®818-UP ratio: Four different weight ratios of TPGS to Plantacare® 818-UP were tried, namely, 0.5:1, 1:1, 2:1, and 4:1.

2.2.1.3. Effect of DEXP incorporation: Two methods were attempted for drug incorporation at a DEXP concentration of 1 mg/mL to mimic the market product: the in-method and the out-method. In the in-method, DEXP was first dissolved in water and then added to the mixture of oil and Smix, while the weighed drug amount was added after ME formation in the out-method.

2.2.2. Characterization of plain and DEXP-ME formulae

2.2.2.1. Clarity and transparency. ME formulae were observed visually for clarity. The ME transparency was confirmed by the determination of the percentage of transmittance (%T) at 650 nm with the aid of a UV–visible spectrophotometer (Shimadzu UV-1601PC UV–Visible Spectrophotometer, Japan) using the continuous phase as a blank (Suthar et al., 2023), noting that none of the individual components have absorption at the selected wavelength.

2.2.2.2. High resolution-transmission electron microscope (HR-TEM) examination. TEM (Jeol 2100 TEM, Japan) was used to visualize the selected ME formulae M9 and DEXP-M9. A volume of 50 µl of ME sample was placed on a carbon-coated grid, left to dry for 3 h then negatively stained with a 1 % w/v aqueous solution of phosphotungstic acid. The sample was viewed under a microscope at an accelerating voltage of 25 kV.

2.2.2.3. 2.2.2.3 Determination of particle size (PS), polydispersity index (PDI), zeta potential (ZP), pH, viscosity, refractive index, conductivity, and type of ME formulae. The size and size distribution of the selected ME formulae were measured relying on the dynamic light scattering (DLS) technique using a Zetasizer (Malvern Instruments Ltd, Malvern, United Kingdom). The samples were properly diluted with a double-distilled water-alcohol system adjusted at a volume ratio of 1:1 for comparative purposes (Schmidt et al., 2021). The size and size distribution of the selected plain and DEXP-loaded formulae were also measured as undiluted samples. All measurements were carried out at a room temperature of 25 ± 0.5 °C. The results were recorded in triplicate for each ME formula. ZP was also determined by laser Doppler anemometry (LDA) using proper zeta cells in a Zetasizer instrument (Malvern Instruments Ltd, Malvern, United Kingdom).

The pH values of selected ME formulae were recorded using a digital pH meter (JENWAY 350, UK) (Hamed et al., 2022). The viscosity was determined using a cone and plate viscometer (Brookfield DV-III ultra-programmable with Brookfield Rheocalc operating software, USA) fitted with a spindle 40 at 100 rpm, adjusted at 25 °C. The refractive index (RI) of ME formulae was determined by a refractometer (Leica Abbe refractometer, Bloomberg, London) at room temperature of 25 °C. The electric conductivity values of the selected formulae were measured by immersing the electrode of a portable digital conductometer (4510 Conductivity Meter, Jenway, London) in a suitable amount of ME formulation kept in a water bath at 25 °C (Wang et al., 2023).

For the determination of the type of the formed MEs, two methods were applied, *viz.,* the dilution test and the dye test. For the dilution test, a representative amount of each ME formula (0.5 mL) was diluted 100-fold with double-distilled water, and the formula was assessed for turbidity, where o/w MEs were easily diluted with water while w/o MEs suffered from turbidity or precipitation. For the dye test, two to three drops of the water-soluble dye, amaranth, were added to the ME to stain the aqueous phase of the formed ME. The oil in water (o/w) MEs were obviously stained with the water-soluble dye, while the continuous phase of the water in oil (w/o) MEs was not stained.

2.2.2.4. Draize eye irritation test. Draize test determines the changes of the cornea in a rabbit eyeball following exposure to a test substance. Two groups (n = 3) were used in this work, and the test was approved by the Research Ethical Committee, Faculty of Pharmacy, Ain Shams University (Approval Number # REC 50). Rabbits were anesthetized using vapors of diethyl ether in a 1 % (w/v) concentration for 5 min, and 100 µl of each tested blank ME (M9 and M11) was applied to the right rabbit eyeball while keeping the left eye as a negative control (Chambers et al., 1993).

Following exposure, the treated eyes were examined at different time intervals (24, 48 and 72 h), and any signs of ocular irritation, including swelling, redness, edema, cloudiness, and hemorrhage, were recorded and scored to evaluate the ocular irritancy. Every visual endpoint has subjective to scoring rules, as shown in Table S1 (Supplementary File). The ocular condition was recorded for the three rabbits treated with the blank ME formulae at different time intervals, and the average score for each Draize endpoint was taken and scored according to the previous table (Chambers et al., 1993).

A rabbit was recorded as positive when corneal opacity of 1 or more, iritis of 1 or more, or conjunctival redness of 2 or more, were maintained at 24, 48 or 72 h after administration. The material is considered a non-irritant when no more than one rabbit is positive, an eye irritant when two or more rabbits are positive but the drawbacks are not severe and symptoms disappear before 7 days, and a severe irritant when two or more rabbits have reactions of corneal opacity of 3 or more and iritis of 2 at 24, 48 or 72 h (Chambers et al., 1993).

2.2.2.5. Histopathological examinations of the treated rabbit eyes. Autopsy samples were taken from the eyes of each group of rabbits treated with the selected plain ME formula and were fixed in 10 % (w/v) formol saline for 24 h. Washing was done with tap water, then successive dilutions of alcohol (ethyl, methyl and absolute ethyl) were used for drying the samples. Samples were clarified in xylene and dipped in paraffin at 56 °C in a hot air oven for 24 h. Paraffin beeswax blocks were set for sectioning at 4-µm thickness by a sludge microtome (Health Care Technologies, Egypt). The obtained tissue sections were placed on glass slides, deparaffinized, and stained with hematoxylin and eosin for evaluation by an optical microscope (Leica microscope, India) (Rizkalla et al., 2011).

2.2.2.6. Fourier Transform Infrared Spectroscopy (FT-IR). Fourier Transform Infrared Spectroscopy (FT-IR) was done using FT-IR apparatus (Nicolet IS10, Thermo Fisher, USA) to demonstrate the compatibility between the drug and the ME components. The analysis was performed for DEXP, double-distilled water, TPGS, Plantacare® 818-UP, Caproyl™ PGMC, and the selected DEXP-loaded ME formula. TPGS and DEXP were analyzed using the potassium bromide (KBr) pellet method, in which the sample was dispersed in KBr and trampled into discs by applying pressure for 5 min in a hydraulic press. For liquid samples, *viz.* double-distilled water, Caproyl™ PGMC, Plantacare® 818-UP, and the selected DEXP-loaded ME formula. KBr powder was impregnated with the solution, left to reach equilibrium for two days, then dried, compressed, and measured. The disc was placed in the path of infrared rays, and the spectrum was documented. The samples were scanned in the wave number range of 4000 to 400 cm^{-1} (Thummajitsakul et al., 2023).

2.2.2.7. Differential scanning calorimetry (DSC). To evaluate the compatibility between the different components of the ME and their thermotropic behavior, DSC analysis was done using a DSC apparatus (DSC-60 Plus, Shimadzu, Japan). For the pure DEXP, an amount of 2–3 mg was directly placed in an aluminum pan. For analyzing the selected ME formulae, a few drops of the formula were added to the pan and were allowed to dry in the air for two days, forming a gel mass due to the presence of TPGS and Plantacare® 818-UP in the formula, which eventually ends in a dried coherent mass containing the drug (Xiong

et al., 2023). The corresponding plain ME formula was also tested for comparison. The experimental conditions of DSC analysis were set constant for all tested samples; the analysis was done under dynamic nitrogen expulsion at 30 mL/min, then the temperature was increased from room temperature to 300 °C at a heating rate of 10 °C/min.

2.2.2.8. Ex-vivo mucoadhesion study. The mucoadhesion properties of the selected blank and DEXP-loaded ME formulae were evaluated using our own-designed balance functioning as a mucoadhesion force measuring device (Abou-ElNour et al., 2020). The mucoadhesion of each tested sample was calculated by measuring the force needed to detach the formula from the freshly excised bovine cornea.

The bovine cornea obtained from a local slaughterhouse was uniformly cut into small circular pieces and kept in sterilized isotonic saline solution until use. The cornea was fixed at the upper stainless-steel stage of the left arm of the modified balance using a glue keeping the epithelial region of the cornea downward. One drop of each sample (10 µl) was installed on the upper surface of the stainless-steel stage of the left arm of the modified balance. The lower stainless-steel stage was vertically raised until the sample touched the lower surface of the cornea's epithelial region, allowing an interaction time of 5 min. Additional water was added in 10 µl increments to a pre-weighed small beaker located on the right side of the modified balance until the formula was detached from the lower surface of the cornea. The quantity of water added was calculated, and the weight of water needed for the detachment of the formula from the cornea was calculated. Each experiment was performed three times (n = 3). The force of detachment (N) in dynes/cm2 was calculated from the following equation:

$$N = m.g / A \quad (1)$$

where m is the weight of water required to detach the formula from the cornea (in grams), g is the acceleration due to gravity (g = 980 cm/s^2), and A is the area of the eye cornea used (in cm^2).

2.2.3. Sterilization of the selected DEXP-ME formula

The selected drug-loaded formula was sterilized using either gamma radiation (Cobalt-60 Gamma Chamber 4000-A, Bhabha Atomic Research Centre, Bombay, India) or aseptic filtration using 0.22 µm Millipore filters. The European Pharmacopoeia has confirmed that 25 KGy of gamma irradiation is a standard dose that guarantees a sterility assurance level (Nguyen et al., 2007). However, two more radiation doses of lower intensities were also tried: 5 and 15 KGy. The chosen formula was stored in separate glass vials and then subjected to the three different doses of radiation using a cobalt-60 gamma chamber 4000-A at a dose rate of 2.08 KGy/h. Another sterilization technique was also implemented, where aseptic double filtration through 0.22 µm Millipore filters was conducted on the selected DEXP-loaded ME formula after being warmed at 38 °C for ease of manipulation.

Following sterilization, the formulae were evaluated for their PS, PDI, and ZP in comparison to the non-sterilized ones. Sterility tests were also conducted to confirm the sterilization of the tested freshly prepared samples by the selected technique, the preservation of sterilization without opening after 6 months, as well as the in-use after opening on a regular basis for 20 s twice daily for one week. This was done by testing the growth of bacteria and fungi in thioglycolate broth and Sabouraud dextrose agar, respectively.

2.2.4. Ex-vivo trans-corneal drug permeation evaluation

The *ex-vivo* permeation was conducted through freshly excised corneas of bovine eyeballs obtained from a local slaughterhouse. The transport of bovine eyeballs and the cornea excision was done within 2 h of the animal's death. The corneal pieces were fixed on our own-designed vertical diffusion chambers with a surface area of 0.63 cm^2 each, made from silicon, in which the epithelial layer was facing the donor compartment. About 900 µl of the tested formula, equivalent to 900 µg DEXP, either as solution or ME formula, was added to the donor compartment. A sample of 1 mL was withdrawn from the receptor compartment occupied with 10 mL of phosphate buffer (pH 7.4) at definite time intervals over 24 h, i.e., 2, 4, 6, 8, 10, 12 and 24 h, and was replaced at each time point with an equal volume of fresh, warm buffer. Samples were analyzed for DEXP content at different time intervals using an HPLC assay.

The whole diffusion chamber was put in a shaking water bath adjusted at 37 ± 0.5 °C. The withdrawn samples were analyzed by the HPLC assay previously described, and the cumulative amounts of drug permeated through the cornea per unit surface area (µg/cm^2) were contrived as a function of time (t) for the selected ME formula compared to the drug solution. The *ex-vivo* corneal permeation evaluation was done in triplicate for each tested formula.

Drug transcorneal flux and permeation rate at steady state, Jss (µg/cm^2/h) was deduced from the slope of the linear graph part. The apparent permeability coefficient (Papp, cm/h) was also calculated by the following equation:

$$Papp = Jss/Co \quad (2)$$

where Co is the initial concentration of drug in the donor compartment.

The DEXP diffusion coefficient, D (cm^2/h), across the excised cornea, was also calculated using Eq. (3):

$$Q = 2\ Co\ (Dt\ /\pi)\ ½ \quad (3)$$

where Q is the cumulative amount of drug released per unit surface area at time t, Co is the initial drug concentration, D is the drug diffusion coefficient, and t is the time. The diffusion coefficient, D, was deduced from the slope of the graph of cumulative DEXP permeated *versus* the square root of time (Gratieri et al., 2011). The enhancement of drug penetration was determined as the enhancement ratio (ER), which was calculated using the following equation (Patel et al., 2010):

$$ER = Jss\ of\ DEXP\text{-}ME/Jss\ of\ DEXP\text{-}solution \quad (4)$$

2.2.4.1. Quantitative analysis of DEXP using HPLC. A previously reported and validated liquid chromatographic method was adopted for the quantitative determination of DEXP using HPLC apparatus (Agilent Technologies 1200 Series, Waldbronn, Germany) with slight modifications. The separation was attained using a C18 column by isocratic elution. A mobile phase consisting of a mixture composed of acetonitrile and phosphate buffer (pH = 3) (25:75, v/v) was used (Saadatmandi et al., 2023). The column effluent was monitored at 232 nm at a flow rate of 1.5 mL/min. No interference of any components of the ME formulation was observed during the elution of DEXP.

2.2.5. Examination of ocular permeation depth using confocal laser scanning microscopy (CLSM)

2.2.5.1. Administration of labeled formulae. The *in vivo* ocular distribution test was conducted on eighteen albino rabbits, each weighing between 2 and 3 kg, bred in the laboratory under identical conditions. The test was approved by the Research Ethical Committee, Faculty of Pharmacy, Ain Shams University (Approval Number # REC 50). Rabbits were anesthetized by vapors of 1 % (w/v) diethyl ether for 5 min. The rabbits were then divided into three groups as follows: treatment group, positive control, and negative control, each of which had six animals. Following anesthesia, 10 µl of the selected ME formula labeled with Rhodamine B (5×10^{-4} mol/L) (Singh et al., 2021) was administered to the rabbit right eye of the treatment group. The positive control group received a solution of the fluorescent dye at the same concentration of 5×10^{-4} mol/L, while the negative control group received only normal saline. Three animals from each group were euthanized after 24 h of

administration, while the other three animals were killed after 72 h, and the rabbit eyes were prepared as will be detailed.

2.2.5.2. Rabbit eye preparation. The right eyes were harvested using scissors, followed by rinsing with phosphate buffer saline (PBS), then immersed in 10 % (w/v) paraformaldehyde at 4 °C for 24 h. The nearby fat was detached from the eyes. The eye cups were then set aside in biopsy cassettes and immersed in acetone for 4 h, followed by xylene for 3 h, and finally placed in paraffin wax kept at 55 °C for 4 h. The paraffin blocks were cut into tiny sections of 5 μm each using a microtome (Health Care Technologies, Egypt), and the sections were placed on glass slides that were slightly warmed for a fraction of time to fix tissue on them. The slides were deparaffinized by dipping them into xylene for 2 min and were visualized using CLSM (SP8 Leica Microsystems Mannheim, Germany) at laser excitation and emission wavelengths of 488 and 532 nm, respectively **(**Fujita et al., 2007**)**. Images were taken at 63X magnification power.

2.2.6. Physical stability of the selected ME formulae

Both plain and DEXP-loaded ME formulae were stored at ambient temperature for six months. These formulae were visually re-inspected, and their PS, PDI, ZP and viscosity were recorded and compared to the initial data after one, three, and six months.

2.2.7. In vivo biological evaluation of the anti-inflammatory activity

2.2.7.1. Endotoxin-induced uveitis (EIU) rat model. The *in vivo* study was conducted on four groups, each composed of four rats, bred in the laboratory under identical conditions. An endotoxin-induced uveitis (EIU) rat model was adopted **(**Chu et al., 2022**)**. The protocol was approved by the Research Ethical Committee, Faculty of Pharmacy, Ain Shams University (Approval Number # REC 50). They were done in cooperation with staff members of the Research Ophthalmology Institute, Giza, Egypt.

Sixteen male albino Wistar rats, 8 weeks old, each weighing approximately 180 ± 20 g, were housed under a 12 h/12 h light and dark cycle in a controlled room temperature of 20–24 °C before the experiment was processed. Lipopolysaccharide (LPS) was injected into twelve animals by sub-plantar injection of endotoxin (100 μg of LPS in 0.1 mL saline) in the right hind paw of each rat.

2.2.7.2. 2.2.7.2 Drug administration. The animals were arbitrarily divided into four groups, each consisting of four rats. Group I was used as a normal negative control, receiving neither an LPS injection nor treatment. Group II was induced by LPS but did not receive any treatment (positive control). Group III received 0.1 % (w/v) DEXP solution, and Group IV received 0.1 % (w/v) DEXP loaded w/o ME (DEXP-M9). A dose of 10 μl of the ME was administered once only to Group IV, while four doses of the same volume of DEXP solution was administered topically every 6 h to Group III. All treatments were instilled into the right eye of the experimental animals after 2 h of endotoxin injection. All groups were sacrificed 24 h from the start of the study **(**Chu et al., 2022**)**.

2.2.7.3. Evaluation of ocular inflammation. Ocular inflammation was evaluated by clinical inspection of the rats, histopathological evaluation, and estimation of the concentration of the inflammatory mediators, interleukin-6 (IL-6) and tumor necrosis factor-α (TNF-α) using the ELISA technique (n = 4).

2.2.7.3.1. Clinical inspection and scoring. Animals were anesthetized 24 h following LPS injection using 1 % diethyl ether (w/v), and the clinical evaluation of the intraocular inflammation was examined by slit lamp biomicroscopy (Goldmann slit microscope, Switzerland). The clinical harshness of ocular inflammation was classified as follows: 0 = no obvious inflammatory reaction; 1 = obvious dilation of the iris and vessels of the conjunctiva; 2 = moderate dilation of the iris and conjunctiva with moderate flare of the anterior chamber; 3 = intense hyperemia in the iris with intense flare in the anterior chamber; 4 = The same clinical signs as 3 in addition to the existence of fibrinoid exudation and miosis.

2.2.7.3.2. Histopathological evaluation. For the microscopic histological evaluation, just after removal of the eyeballs, the eyeballs were immersed in cold 10 % (w/v) formaldehyde for at least 12 h. The specimens were then dried through ascending grades of ethyl alcohol with the following concentrations: 30, 50, 70, 90, and finally 96 % (w/v). Paraffin beeswax blocks were made for sectioning at 4-μm thickness by a sludge microtome (Health Care Technologies, Egypt), followed by further drying in absolute alcohol for histological evaluation by staining using hematoxylin and eosin (H&E) **(Bancroft & Layton, 2012;** Yadav & Ramana, 2019**)**.

Evaluation of the anterior eye segments takes place for the iris, ciliary body and the corneal tissue was scored as follows: 0 = normal tissue; non-keratinized stratified squamous epithelium of the cornea with no inflammatory cells in the iris or ciliary body, 1 + = thickened iris stroma with secretions and dilated iris vessels with protein, and/or a few scattered inflammatory cells, 2+ = penetration of inflammatory cells into the ciliary body and/or stroma of the iris, with a moderate number of inflammatory cells within the anterior chamber, 3+ = heavy penetration of the inflammatory cells within the ciliary body and iris stroma and a heavy penetration of inflammatory cells within the anterior chamber, and 4+ = heavy exudate from cells with thick protein aggregation in the anterior chamber and inflammatory cell deposition within the corneal endothelium. Both eyes were graded separately in a blind fashion, then averaged.

2.2.7.3.3. Quantitative determination of IL-6 and TNF- level. The IL-6 and TNF-α concentrations were quantitatively determined in the aqueous humor samples of rats after proper dilution using rat IL-6 and TNF-α ELISA kits in a sandwich ELISA technique (single-wash 90-minute ElISA technique for IL-6 and 3.5-h assay for TNF-, respectively) **(**Shi et al., 2021**)**.

2.2.8. Statistical analysis

All *in vitro*, *ex vivo*, and *in vivo* experimental results were reported as the mean of three determinations ± standard deviation (SD). A *t*-test (student's *t* test) was conducted to compare two different parameters, while the data obtained from different groups was compared using one-way analysis of variance (ANOVA). The significance of the difference between formulae was calculated by Tukey Kramer multiple comparison using Graph Pad Instate® software. The statistical significance level (P) value was set at ≤ 0.05.

3. Results and discussion

3.1. TPGS/Plantacare®-based MEs

In this work, attempts were made to prepare the ME relying on the use of the novel SAA combination, made from TPGS and Plantacare®, with the unique properties of the oil Capryol™ PGMC without any additional co-SAA. Capryol ™ PGMC was thought to enhance the stability of the formed ME by virtue of its co-SAA properties **(**Rehman et al., 2022**)**.

3.2. Optimization of TPGS/Plantacare®-based MEs

3.2.1. Effect of Plantacare® type

The phase diagrams of the systems prepared with both types of Plantacare®, 1200 and 818U, are illustrated in Fig. S1 **(**Supplementary File**)**. Formulae denoted by Q and L were taken from the areas representing the one-phase systems from Plantacare® 1200 and 818-UP, respectively, and some of them were characterized as shown in **Tables S2 and S3 (**Supplementary File**)**. It is obvious that the area representing the one-phase system in the diagram constructed with

Plantacare® 818-UP, Fig. S1**(b)** was larger compared to that obtained with Plantacare® 1200, Fig. S1**(a)**. All formulae prepared with Plantacare® 1200, Table S2, scored large droplet size ranging from 643 nm to 3.98 μm and were stable for one day only and up to one week (Q11). Formulae prepared with Plantacare®818-UP, Table S3, scored PS varying from 430 nm to 3.4 μm. Worthy to mention that we used a 1:1 water/alcohol mixture for dilution during PS analysis at this preliminary optimization step. This mixture was suitable for all MEs obtained in this work even the highly viscous ones. The prepared formulae were stable for one day (L15) and up to two weeks (L7 and *L*10), depending on the composition and oil content. Formulae prepared at high SAA concentration > 60 % (w/w); Q11 and L7 from the two-phase diagrams, TPGS: Plantacare® 1200; 1:1, and TPGS: Plantacare® 818-UP; 1:1, respectively, formed a jellified mass and showed relatively higher stability compared to the other formulae owing to the gel-forming ability of TPGS manifested at high concentrations.

Furthermore, at a similar composition, formulae prepared with Plantacare®818-UP scored smaller size compared to their counterparts prepared with Plantacare® 1200. For instance, significant differences ($p < 0.05$) were evident between formulae L1 (913 ± 70 nm) and Q1 (1668 ± 1997 nm); L-7 (430 ± 40 nm) and Q11 (2527 ± 1345 nm); and finally, formulae *L*10 (464 ± 60 nm) and Q14 (643 ± 248 nm). This may be attributed to the smaller carbon chain of Plantacare® 818-UP; C8-C16 alkyl glycosides, compared to Plantacare®1200; C12-C16 **(**Keck et al., 2014; Pantelic & Cuckovic, 2014**)**. Based on the obtained results, Plantacare® 818-UP was chosen for subsequent experiments.

3.2.2. *Effect of TPGS: Plantacare® 818-UP mass ratio*

Fig. 1 shows that a one-phase region can be seen in the phase diagram of each of the four TPGS: Plantacare®818-UP ratios, with the smallest area obtained with the 4:1 ratio containing the highest TPGS concentration. Despite the large ME area formed in the case of TPGS: Plantacare® 818-UP mass ratios of 0.5:1 and 1:1 ratio, yet the majority of the ME formulae exhibited very limited stability profiles for a period ranging from one day to a maximum of two weeks, as shown in Tables S4 and S3 **(**Supplementary File**)**, respectively. This denoted the instability of the SAA film formed at the oil–water interface, leading to the coalescence of the oil droplets. Despite the use of Caproyl™ PGMC, characterized by its Co-SAA property, its concentration was probably insufficient to provide the optimal flexibility for the SAA film **(**Rehman et al., 2022**)**. This is in addition to the low concentration of TPGS needed to impart viscosity and provide stability to the prepared ME for a long period of time. It is worthy to mention that at all Smix ratios used, a gel-like viscous system was formed at higher Smix concentrations > 50 % owing to the gel-forming ability of TPGS **(**Telò et al., 2017**)**. Using TPGS: Plantacare 818-UP mass ratios of 2:1 (Table 1.) and 4:1 (Table S5 - Supplementary File) resulted in formulae within the monophasic area with varying stability profiles, ranging from one day up to a maximum of 6 months. The presence of a relatively high concentration of TPGS acquiring gelling property in the presence of an aqueous medium led to relatively higher stability compared to the previous two ratios.

All formulae prepared with TPGS: Plantacare® 818-UP 1:1, Table S3 **(Supplementary File)**; scored PS larger than 400 nm with PDI ranging

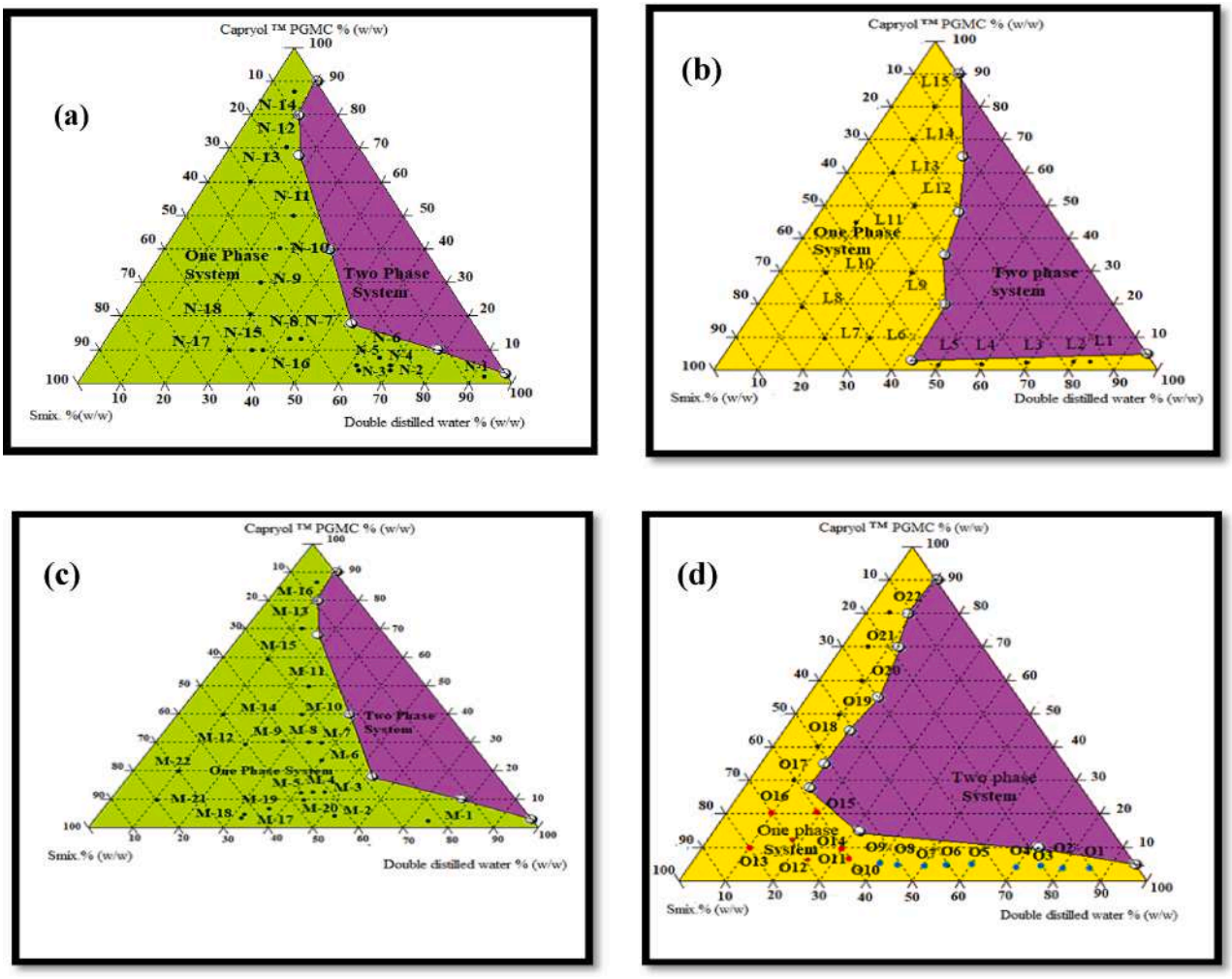

Fig. 1. Pseudo-ternary phase diagram showing the different regions obtained for the systems composed of Caproyl™ PGMC and TPGS: Plantacare® 818-UP, (a) 0.5:1, (b) 1:1, (c) 2:1, and (d) 4:1.

Table 1
Characteristics of formulae prepared with TPGS: Plantacare® 818-UP at 2:1 (w/w).

Formula code	Compositions (%wt)			Suggested System[#]	Results* ± SD			Stability Duration (Appearance)
	Capryol oil	Smix	Water		PS* (nm) ± SD	PDI* ± SD	ZP* (mV) ± SD	
M1	2.50	25.2	72.3	o/w ME	18 ± 2	0.20 ± 0.01	−18 ± 4	Three months (Clear transparent)
M2	3.30	43.11	53.59		120 ± 3	0.20 ± 0.02	−16 ± 2	Three days only (Clear transparent)
M3	12.50	40.80	46.70		44 ± 1	0.40 ± 0.30	−12 ± 3	One month (Clear transparent)
M4	12.50	44.20	43.30		83 ± 3	0.40 ± 0.02	−15 ± 3	One month (Clear transparent)
M5	12.50	47.60	39.90		314 ± 2	0.8 ± 0.10	−13 ± 2	One month (Clear transparent)
M6	25	37.40	37.60	w/o ME	14 ± 1	0.30 ± 0.01	−12 ± 1	One month (Clear transparent)
M7	30	34	36		12 ± 2	0.40 ± 0.02	−14 ± 2	14 days (Clear transparent)
M8	30	37.40	32.60		12 ± 2	0.20 ± 0.02	−12 ± 2	One month (Clear transparent)
M9	30	40.80	29.20		18 ± 2	0.30 ± 0.02	−12 ± 2	Six months (Clear transparent)
M10	40	34	26		22 ± 3	0.30 ± 0.02	−10 ± 0.1	Six months (Clear transparent)
M11	50	27.20	22.80		30 ± 1	0.3 ± 0.02	−10 ± 4	Six months (Clear transparent)
M12	30	50	20		102 ± 14	0.26 ± 0.03	−12 ± 2	One month (Clear transparent)
M13	70	17	13		450 ± 3	0.30 ± 0.01	−8 ± 0.2	One week (Clear transparent)
M14	40	50	10		137 ± 20	0.40 ± 0.02	−16 ± 2	One month (Clear transparent)
M15	60	30	10		230 ± 10	0.30 ± 0.05	−14 ± 3	One week (Clear transparent)
M16	85	5.44	9.56		600 ± 5	0.30 ± 0.01	−12 ± 0.2	Three days only (Clear transparent)
M17	3	64.60	32.40	Gel-like ME	280 ± 4	0.40 ± 0.02	− 14 ± 2	Six months (Clear viscous gel)
M18	4	63.92	32.08		330 ± 3	0.50 ± 0.10	−14 ± 3	
M19	5	54.40	40.60		350 ± 3	0.40 ± 0.02	−16 ± 2	
M20	10	47.60	42.40		420 ± 2	0.60 ± 0.10	−14 ± 2	
M21	10	80	10		289 ± 20	0.50 ± 0.04	−16 ± 2	
M22	20	70	10		352 ± 40	0.40 ± 0.05	−12 ± 2	

*Average of three determinations performed on diluted ME; 1:1water: alcohol system, PS: particle size, PDI: polydispersity index, ZP: zeta potential and, SD: standard deviation. [#] The suggested ME type is based on the results of dilution and dye tests. N.B All formulae were measured after dilution by water: ethanol mixture in a ratio of 1:1(w/w).

from 0.5 to 1 and low ZP not exceeding −12 mV. Meanwhile, formulae prepared with TPGS: Plantacare® 818-UP 4:1, collected in Table S5 **(**Supplementary File**)**, scored larger PS compared to those prepared with TPGS: Plantacare® 818-UP 0.5:1. A high concentration of Plantacare®818-UP probably enhanced the emulsification. Formulae prepared at the ratio 2:1 scored smaller droplet size and higher stability compared to those prepared at the ratio 0.5:1, as evidenced by comparing M9, M10 and M11, with respective droplet size of 18 ± 2, 22 ± 3 and 30 ± 1 nm (Table 1), to their counterparts prepared with the ratio 0.5:1, N9, N10 and N11, with respective droplet size of 83 ± 4, 176 ± 14 and 61 ± 3 nm ($p < 0.05$) (Table S4 - Supplementary File). This can be attributed to the optimum system viscosity caused by TPGS, which decreased the tendency of coalescence of internal phase droplets, which in turn improved the stability of the formed ME systems. Based on the large droplet size of the formulae formed at TPGS: Plantacare® 818-UP 4:1 and 1:1 and the limited stability of formulae prepared at TPGS: Plantacare® 818-UP 0.5:1, these ratios were excluded from subsequent works. Formulae prepared at the ratio 2:1 scored the smallest droplet size and highest stability among the tested ratios.

ME formation and droplet size are greatly affected by the SAA film curvature at the oil–water interfaces, which could be elucidated by the concept of the critical packing parameter (CPP). The CPP can be calculated using the equation: CPP = v/lc.ao, where v is the hydrophobic group volume of the SAA, lc is the critical hydrophobic chain length of the SAA, and ao is the cross-sectional area of the hydrophilic head group of the SAA. The spontaneous curvature of the surfactant monolayer (Ho) is another phenomenon related to the SAA film formed at the oil–water interfaces. This curvature depends on both the composition of the two phases it separates and the SAA type **(**Eastoe et al., 1997; Cho et al., 2008; Eastoe et al., 2013**)**.

The formation of o/w MEs is favorable if the effective polar part of SAA is bulkier than the hydrophobic portion (ao > v/lc), and hence the interface curves spontaneously towards water (positive curvature Ho). For the w/o MEs, the interface curve is in the opposite direction as ao < v/lc, and it curves spontaneously towards oil (negative Ho). When ao ≈ v/lc, the curvature assumes a zero value, indicating the formation of a lamellar liquid crystal depending on the rigidity of the film. The increase in the TPGS proportion of Smix 2:1 is expected to cause a reduction in the critical hydrophobic chain length of the SAA (lc) compared to the lower mass ratio of 0.5:1, owing to the bulky aromatic structure of tocopherol succinate. Moreover, the linearity of the flexible and hydrophilic PEG 1000 chains in TPGS could be the second reason based on their high capacity to coil and stretch, expecting to increase the cross-sectional area (ao) of the SAA head groups at the higher Smix of 2:1 **(**De Caro et al., 2023**)**. Since polyalkyl glycosides such as Plantacare® 818-UP are bulky-structured SAAs, they are estimated to increase the interfacial fluidity and flexibility by penetrating between TPGS molecules located at the oil–water interface, creating a disordered film, and forming void spaces within its structure. This eventually leads to an increase in the cross-sectional area head group per SAA (ao) in favor of

v/lc, thus tending to the formation of isotropic o/w MEs, typically at low oil content.

Indeed, the formation of ME requires a considerably low oil–water interfacial tension (γo/w). The typical SAAs are often not capable of reaching such low γo/w values, and for this reason, the addition of a Co-SAA is often mandatory. However, at the non-polar side of the interface, it is reported that the oil molecules, particularly those of short chains, are capable of piercing to some extent between the SAA hydrocarbon tails. The penetration of oil molecules is also reported to depend on the chemical structures of SAAs. The dissimilar architectures of hydrophobic moieties in both SAAs would result in a more disordered film at the interface, thus providing a space for oil penetration and mixing. These facts matched well with both TPGS and Plantacare®818-UP in our novel system.

Therefore, at higher oil concentrations, the linear oil structure (Capryol™ PGMC) was assumed to locate among the SAA hydrocarbon chains, causing an elevation of both (v) and (lc) of the hydrophobic portions, hence ao < v/lc, translated by the successful formation of w/o MEs. The deeper the oil penetration, the more curvature is enforced towards the polar side, resulting in a negative curvature towards the water, hence a decrease in Ho. This case is typical for Capryol ™ PGMC used in the present system, which is considered a medium-chain oil of C8 carbon chain length and supposed to mix well with the hydrophobic SAA molecules, imparting more elasticity to the film formed at the water–oil interface, lowering γo/w efficiently, and thus acting as a Co-SAA.

Based on the results and observations, we can deduce the superiority of the w/o ME formulae, M9 and M11, composed of 30 and 50 % w/w of oil, 40.8 and 27.2 % w/w of Smix, and 29.2 and 22.8 %w/w of water, respectively, in terms of their stability and characteristics. Both formulae retained their transparency during the entire storage period of six months. The droplet sizes, PDI, and ZP of the selected blank formulae M9 and M11 were re-measured without dilution, just to confirm the actual ME parameters, and they showed appropriate values of 32 ± 5 and 45 ± 7 nm, 0.3 ± 0.05 and 0.4 ± 0.15, −12 ± 3 and −10 ± 2 mV, respectively. Hence, they were chosen for further ocular irritation testing.

3.3. Draize eye irritation test and histopathological examination

Visual examination of the rabbit's eye treated with formula M9, Fig. S2**(b)** revealed no redness, swelling, or closure of the eye during the whole experiment. A result similar to that obtained with the left eyeball (negative control), Fig. S2**(a)**. Conversely, the eye treated with formula M11 revealed visible signs of irritation, Fig. S2**(c)**.

The ocular condition was recorded for each of the three rabbits of the same group at different time intervals: 24, 48 and 72 h, and the average score for each Draize endpoint was calculated according to Table S1 as follows: for M9, 0 degree of ulceration, 0 hyperimea and swelling, and 0 for inflammation of the conjunctiva, while for M11, 0 degree of ulceration, 1 hyperimea and swelling, and 2 for inflammation of the conjunctiva, and these scores lasted during the whole experiment (72 h). Hence, M9 can be considered a non-irritant according to the reported scoring system **(**Chambers et al., 1993**)**.

The rabbit eyes treated with formulae M9 and M11 for 72 h were dissected and prepared for histopathological examination. The left rabbit eyeball was also examined as a negative control. The histological structures of the rabbit's cornea and conjunctiva are illustrated in Fig. 2. The control eye shows no histopathological alterations, demonstrating normal histological structures; the outer epithelium, inner endothelium, and intermediate stroma were the three layers that made up the stroma. Bowman's membrane maintained a non-keratinized, stratified squamous epithelium on the cornea. The stroma was made up of continuous lamellae of uniformly thick acidophilic collagenous fibers. Keratocytes were flattened cells dispersed between the stromal lamellae in the ground material. The cornea's inner endothelium was made up of a single layer of flattened cells held together by a thick, homogeneous

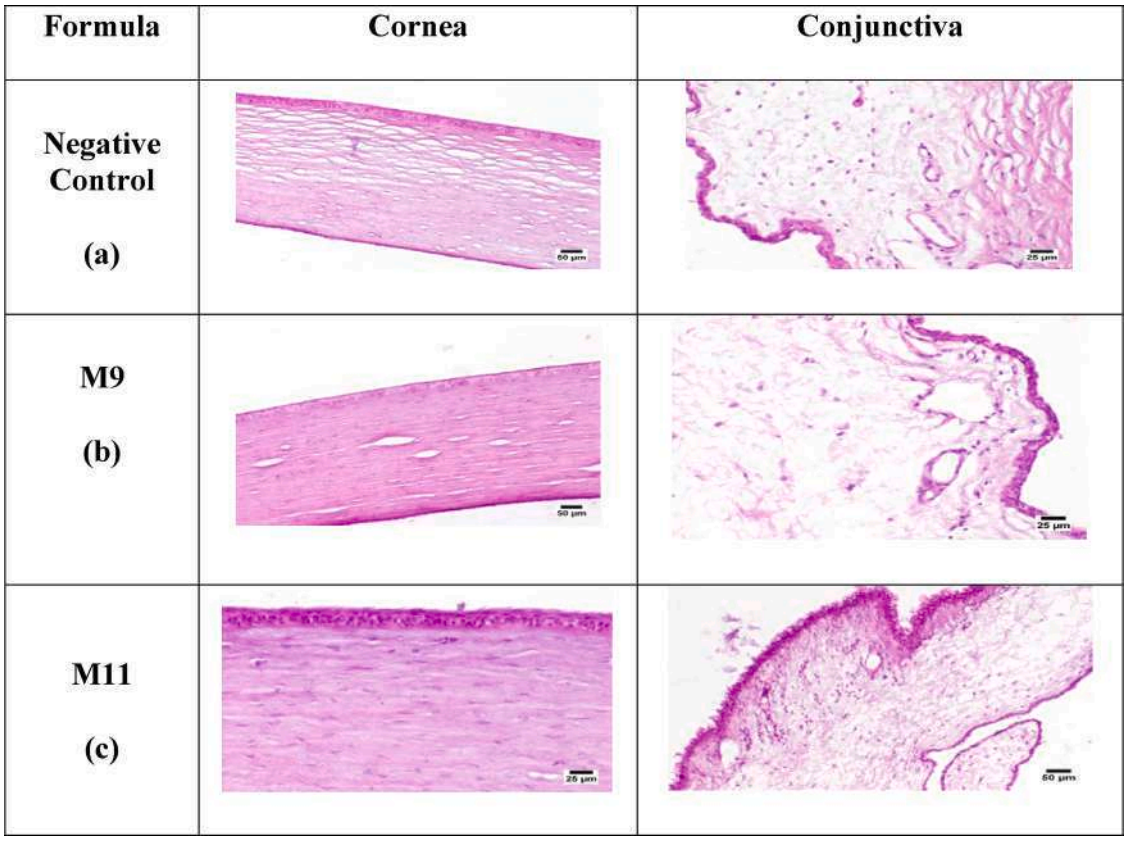

Fig. 2. Histopathological images of the cornea and conjunctiva of rabbit eyes; (a) negative control and groups treated with (b) M9 and (c) M11.

Descemet's membrane. The different eye sections treated with M9 are displayed in Fig. 2**(b)**, do not show any histopathological changes, while the rabbit eyes instilled with M11, Fig. 2**(c)**, reveals a focal stratification in the corneal surface epithelium of the rabbit eye with congestion in the underlying blood vessels, which indicates inflammation of the rabbit's eye **(**Daston & Freeberg, 2020; Ramos et al., 2017**)**. These results were in agreement with those obtained from the Draize test.

The obtained results confirmed the convenience of TPGS for ocular use at concentration reaching 30 % (w/w) and warranted the safety of alkyl glycosides as biocompatible SAAs used in eye preparations up to 40 % (w/w). Hence, it can be deduced that although the lower Smix percentage, increased the concentration of Capryol™ PGMC from 30 % (w/w) in M9 to 50 % (w/w) in M11, this led to the occurrence of ocular irritation. This is attributed to the previously reported concentration-dependent cytotoxicity of the oil **(**Ujhelyi et al., 2012**)**. Based on the above results, the w/o ME formula M9 was chosen for subsequent experiments.

3.4. Preparation of DEXP-loaded TPGS/Plantacare®-based MEs

Attempts to incorporate the drug using various methods revealed the superiority of the out-method where DEXP (1 mg/mL) was incorporated following ME formation. Moreover, no drug precipitation was seen upon increasing the drug concentration to 50 mg/ml while applying the out-method. Conversely, the addition of DEXP before the formation of the ME in the in-method resulted in drug precipitation and obvious turbidity. It can thus be inferred that the ME system should be formed and stabilized by SAAs first before the addition of the drug, as the latter, being a salt, may cause a kind of destabilization of the ME if added initially before ME formation **(**Kabalnov et al., 1995**)**.

The results also demonstrated the capacity of the selected w/o ME to incorporate large amounts of the water-soluble drug, confirming its suitability for entrapping any hydrophilic actives even in large doses. This could be attributed to the emulsifying power of both TPGS and Plantacare® 818-UP in addition to the special Co-SAA properties of Capryol ™ PGMC. A DEXP concentration of 1 mg/mL was maintained in all subsequent studies as it mimics the drug concentration in DEXP-containing marketed eye products.

3.5. Characterization of the selected plain and DEXP-loaded ME formulae

3.5.1. ME physico-chemical characterization

The isotropicity of the developed MEs was confirmed by measuring percent transmittance (%T); the results showed high %T values that approached 100 %, 99 %, and 98 % for plain and drug-loaded formulae, respectively. Table 2 shows that the droplet size of the selected DEXP-loaded ME formula, DEXP-M9, did not significantly differ from the plain one ($p > 0.05$), with respective values of 43 ± 5 and 32 ± 5 nm. The developed MEs also showed a narrow droplet size distribution (PDI ≤ 0.35) with a non-significant difference between plain and drug-loaded formulae ($p > 0.05$) and relatively high charge magnitudes of −12 mV with an insignificant difference between them ($p > 0.05$), delineating the potential stability of the prepared systems **(**Moghimipour et al., 2013**)**. TEM images of both plain M9 and drug-loaded DEXP-M9 formulae, Fig. 3**(A)**, revealed discrete spherical particles. Smaller water droplets were obtained with M9 compared to DEXP-M9. It should be mentioned that the size in TEM images was slightly higher than that obtained by DLS, which may be attributed to the drying process of the w/o formulae before measurement.

The pH value for both plain and drug-loaded formulae was almost neutral, ranging from 6.7 to 6.8, revealing that the inclusion of DEXP salt did not significantly alter the final pH of ME ($p > 0.05$). These data ensure the safety of the prepared MEs without any potential ocular irritation or discomfort. The measured viscosities of the prepared MEs, either plain or drug-loaded, scored 147 ± 5 and 150 ± 7 cP, respectively, with an insignificant difference between them ($p > 0.05$). The observed high viscosity was referred to the presence of both TPGS and Plantacare® 818-UP at high Smix concentration exceeding 40 % w/w in addition to the viscous oil Capryol™ PGMC. The relatively high viscosity is needed to increase the stability of ocular preparations by preventing *in vitro* drug precipitation and increase the bioavailability by increasing the retention and adhesion of the formula to the ocular surface **(**Elmotasem & Awad, 2020**)**. Both ME formulae (plain and drug-loaded) showed comparable RI values of 1.436 ± 0.030 and 1.439 ± 0.020, respectively, with a non-significant difference ($p > 0.05$). The findings match well with the results of similar nano-emulsifying drug delivery systems **(**Shakeel et al., 2021**)**, proving the w/o type of the developed ME and demonstrating the isotropic behavior of ME as well.

The conductivity results of the prepared w/o MEs reached values of 0.15 and 0.16 μS/cm in the case of plain and drug-loaded formulae, with an insignificant difference among them ($p > 0.05$). The typical conductivity of non-polar solvents such as oils usually scores values in the range (10^{-9} – 0.1^{-9} S/m) and polar solvents such as water (0.3 – 84 S/m). Clausse et al. described the ME conducting system as a percolating system that is characterized by a rapid change in conductivity as a function of water volume fraction above a critical value **(**Clausse et al., 1983**)**. The sharp increase in conductivity above that value is attributed to water percolation or transition over the oil-rich side. Below the percolation transition, the conductivity of the w/o ME keeps lowering with the decreasing volume fraction of water but is still much higher than the typical conductivity of a non-polar solvent. This can be elucidated by the fact that nanodroplets carry positive or negative charges. The translocation of these charged droplets in an electric field will cause a finite conductivity whose magnitude is immediately related to the average charge on a droplet **(**Clausse et al., 1983**)**.

3.5.2. Fourier Transform Infrared Spectroscopy (FT-IR)

The FT-IR spectra of different ME components as well as the DEXP-loaded ME formula, DEXP-M9, are illustrated in Fig. 3 **(B)**. The FT-IR spectrum of water (a) showed a characteristic band at 3447.58 cm^{-1} due to the –OH group. A sequence of bands appeared in TPGS spectrum (b) at different wave numbers: 2892.52, 1735.36, and 1466.72 cm^{-1} for the –CH aliphatic, C = O, and aromatic ring, respectively. Plantacare® 818-UP spectrum (c) revealed different bands at 3404.82 cm^{-1} due to the –OH group, 2924.27 cm^{-1} of the –CH group, and 1648.04 cm^{-1} due to the $–CH_2$ aliphatic. Capryol ™ PGMC (d) exhibited comparable

Table 2
Physical characterization of the selected plain and drug-loaded w/o ME formulae.

Formula	Results* ± SD						
	PS (nm)	PDI	ZP (mV)	pH	Viscosity (cP)	RI	Conductivity (μS/cm)
Plain w/o ME (M9)	32 ± 5	0.30 ± 0.05	−12 ± 3	6.70 ± 0.1	147 ± 5	1.436 ± 0.030	0.15 ± 0.01
Drug loaded w/o ME (DEXP-M9)	43 ± 5	0.35 ± 0.07	−12 ± 4	6.80 ± 0.2	150 ± 7	1.439 ± 0.020	0.16 ± 0.01

*Average of three determinations performed on selected ME formulae. SD: standard deviation, PS: particle size, PDI: polydispersity index, ZP: zeta potential, RI: refractive index. N.B All formulae were measured as undiluted samples.

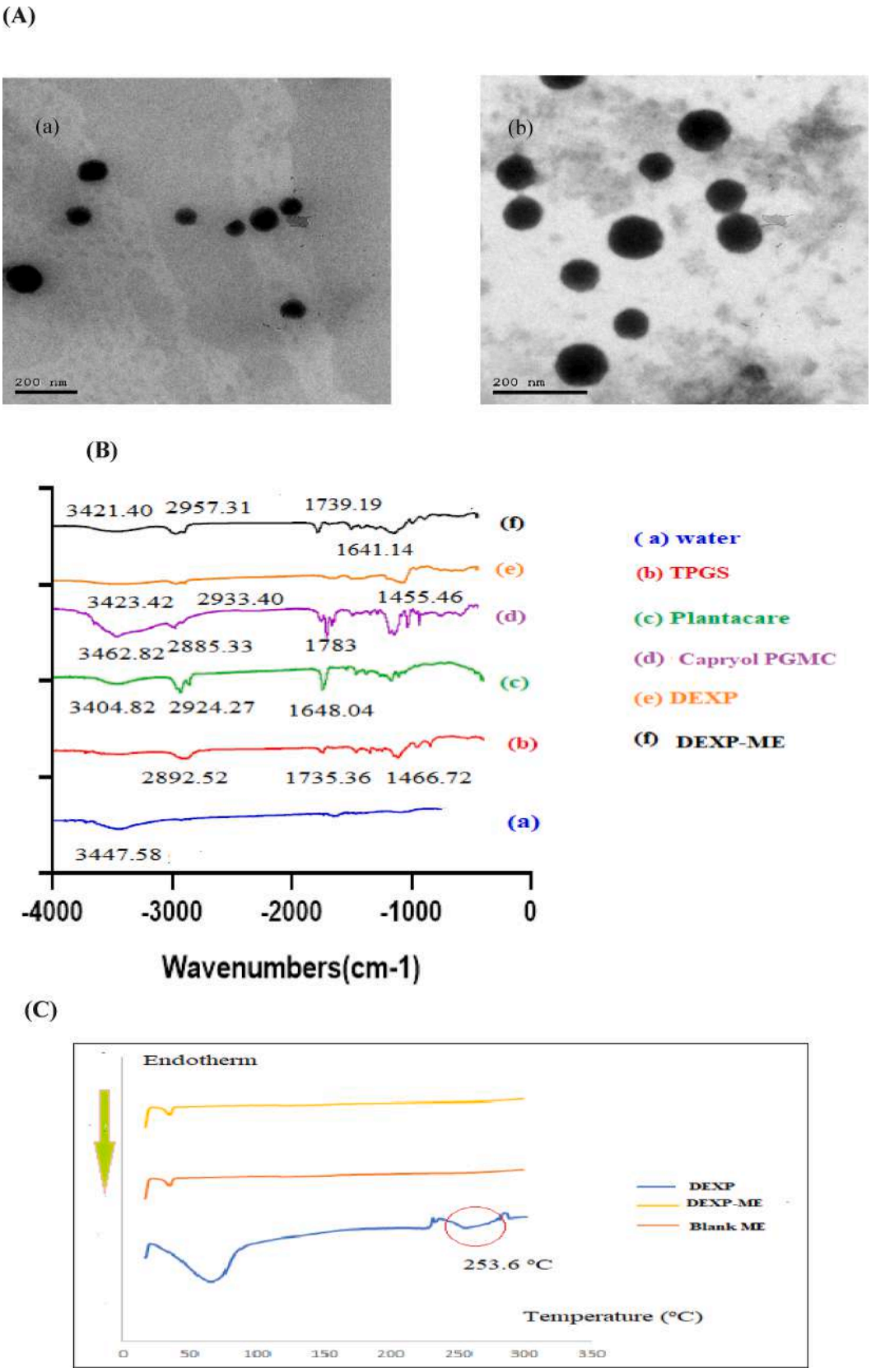

Fig. 3. *In vitro* characterization of the selected MEs: (A) HR-TEM images of the selected w/o ME formulae, (a) plain M9, and (b) drug- loaded DEXP-M9 at different magnifications. (B) FT-IR spectra representing different ME components and DEXP-M9. (C) DSC thermograms of DEXP, plain ME (M9), and drug-loaded formulation (DEXP-M9).

wavenumbers of similar groups; its spectrum showed bands at 3462.82, 2885.33, and 1738 cm^{-1}, which belong to the –OH group, –CH aliphatic, and C = O of caprylic acid and propylene glycol, as previously stated. The FT-IR spectrum of DEXP (e) showed different bands at various wavenumbers; a broad peak appeared at 3423.42 cm^{-1} matched to the –OH group, 2933.40 cm^{-1} to the –CH group, and a sharp band at 1455.46 cm^{-1} due to the aromatic ring (Ajaz et al., 2020). The spectrum of the DEXP-loaded ME formula, DEXP-M9 (f), demonstrated a combination of all the individual components described before. It showed several respective bands at different positions: 3421.40, 2957.31, 1739.19, and 1641.14 cm^{-1} belonging to –OH, –CH, C = O, and $–CH_2$ groups, which match well with the groups already present in each of the ME components, endorsing their compatibility.

3.5.3. Differential scanning calorimetry (DSC)

As observed in Fig. 3**(C)**, the drug thermogram was typical with two endothermic peaks: one at 253.6 °C corresponding to its reported melting point, and the other around 100 °C corresponding to the evaporation of adsorbed water. The DSC thermogram of the drug-loaded ME, DEXP-M9, showed a small endothermic peak corresponding to the melting of TPGS at around 40 °C comparable to that of the blank M9 formula with no evidence of a drug peak, which indicates complete amorphization and solubilization of the drug in ME. This may be attributed to the gel formation of the ME upon drying, which eventually ends with the formation of a dried coherent mass, that retains the drug within its structure and prevents its precipitation (Siafaka et al., 2023).

3.5.4. Ex-vivo mucoadhesion study

The mucoadhesive characteristic of the applied formulae is of critical value for their successful ocular delivery. This property prevents the leakage of the applied formulation and hence allows the prolongation of drug residence time within the eye, which enhances DEXP's anti-inflammatory effect for efficient ocular treatment. The mucoadhesive properties of both plain M9 and DEXP-M9 ME formulae were tested by determining the force of detachment required to detach each formula from the freshly excised bovine cornea.

The larger the force of detachment, the stronger the mucoadhesive property of the tested formulation. The force of detachment values of plain and DEXP-loaded ME formulae attained 731.34 ± 50 and 887 ± 67 dynes/cm^2, respectively. This high force of detachment could be attributed to the proven high viscosity of these formulae. The effect of viscosity on the formulation's mucoadhesive property was previously reported. Moreover, both SAAs, the vitamin E derivative 'TPGS' and the polysaccharide derivative 'Plantacare®', were reported to enhance mucoadhesion by allowing contact with the mucin of the corneal tissues *via* electrostatic interactions (de Oliveira Cardoso et al., 2020).

3.6. Sterilization and sterility test

Sterilization was conducted using gamma irradiation at three different doses: 5, 15, and 25 KGy. Table S6 (Supplementary File) summarizes the characterization results before and after irradiation. Despite the documented decrease in PS of MEs following gamma radiation, yet the droplet size and size heterogeneity in plain and drug-loaded formulae increased significantly at the three radiation doses ($p < 0.05$) while the surface charge magnitudes were reduced ($p < 0.05$) as shown in Table S6 (Supplementary file). This could be attributed to the elevated oil content, where beta-oxidation of the oil would take place, in addition to the prospective drug degradation (Guo et al., 2017).

Another sterilization technique was then applied using aseptic filtration using 0.22 μm Millipore filters. Table S7 (Supplementary File) shows the characterization results of the plain and DEXP-loaded MEs before and after aseptic filtration. As seen from Table S7 (Supplementary file), significant declines ($p < 0.05$) in both PS and PDI were noted, with a non-significant effect ($p > 0.05$) on the surface charge magnitudes for plain and drug-loaded formulae, respectively. The reduction of ME droplet size following sterilization may be attributed to the removal of any possible aggregates present, and the possible extrusion effect of filtration technique on the ME droplets, in addition to the 'de-dusting effect' where removal of the very fine particles was reported to enhance the physical stability affecting the whole z-average of ME droplets measured by the DLS (Law & Britton, 2012; Zheng et al., 2013). Therefore, the aseptic filtration technique was adopted for sterilizing DEXP-loaded ME in all subsequent experiments. The sterility of the tested samples has been proven, as no bacterial or fungal growth was detected in neither the thioglycolate broth nor the Sabouraud dextrose agar. Moreover, the conservation of sterility for a 6-month storage period without opening and after in-use for one week was ascertained for samples sterilized by aseptic filtration by the same microbiological tests described before.

3.7. Ex-vivo trans-corneal drug permeation evaluation

DEXP permeation across excised bovine cornea was studied from both aseptically filtered and non-filtered ME, and the results were compared to those obtained with an aqueous solution prepared at the same drug concentration (0.1 % w/v) in phosphate buffer (pH 7.4) for 24 h, Fig. 4. It could be clearly seen that the drug permeation from the solution was relatively much lower than the corresponding ME formula, either non-sterilized or aseptically filtered. This was attributed to the hydrophilic nature of the drug salt, which could not permeate through the lipid nature of the corneal tissues. On the contrary, enhanced drug permeation through the corneas was noted in the case of the ME because of its high oil content (30 %), which is biocompatible with the hydrophobic cornea, added to the existence of large amounts of SAAs, which enhanced the drug permeation through the eye cornea.

As shown in Fig. 4, only 77.39 μg/cm^2 equivalent to about 5 % of DEXP, was permeated in the case of the aqueous solution after 2 h, while a significantly higher increase in the amount permeated per unit area ($p < 0.05$) reached 4-fold in the case of the ME formula. There was an insignificant difference in the amount permeated per unit area between the non-sterilized ME and the sterilized ME by aseptic filtration ($p > 0.05$). Finally, the drug was completely permeated after 24 h from both the selected ME formula and the aseptically sterilized formula, compared to only 27 % for the solution. The higher drug permeation from ME formulae will eventually lead to higher drug bioavailability and, hence, better therapeutic outcomes.

Different parameters were assessed for both the ME formulae, either non-sterilized or aseptically filtered, and the aqueous solution, namely, the drug flux, permeability, and diffusion coefficients.

As seen from Fig. 4, the drug flux from ME formulae, either sterilized or not, reached its maximum after 8 h, then a reduced permeation rate was observed, forming a biphasic permeation profile. The higher earlier permeation rate could be attributed to the high concentration gradient which affects the overall permeation profile (Shahab et al., 2020). Different permeation parameters were then calculated for the linear portion of the curve, and the data were collected in Table 3. It could be noticed from Table 3 that the flux from the ME formula, either sterilized or not, was four-fold higher than that of aqueous solution during the initial permeation phase. Moreover, higher permeability and diffusion coefficients were obtained for all tested formulations. This may be attributed to the presence of a large amount of SAA, which increases the permeation and diffusion of the drug and subsequently leads to a higher flux of the selected ME formula (Al Saqr et al., 2023). In addition, the permeability enhancement in the case of the ME formula was mostly due to its lower droplet sizes, as presented before.

3.8. Ocular permeation using CLSM

As observed from the CLSM images, a strong fluorescence was perceived in the cornea, conjunctiva, and retina treated with the labeled ME compared to the labeled solution after 24 and 72 h, as shown in

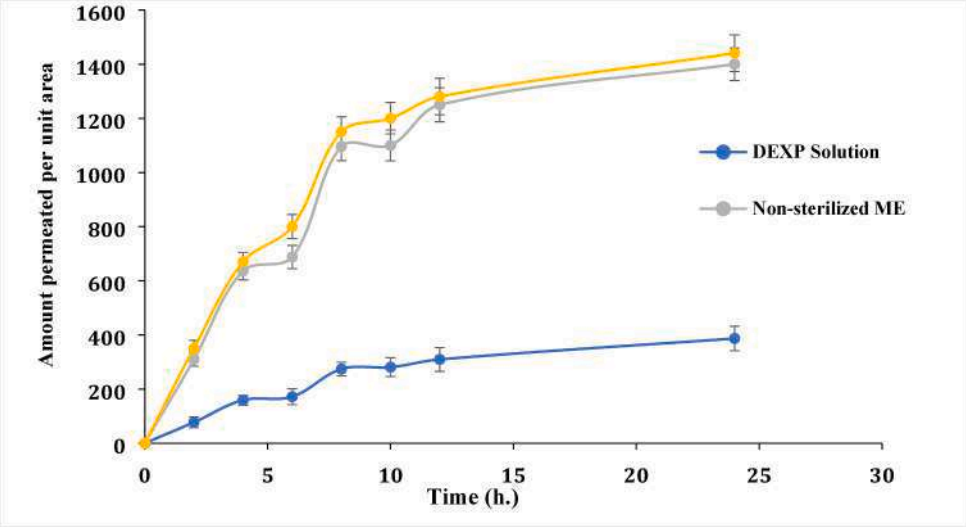

Fig. 4. Trans-corneal DEXP permeation profiles from loaded w/o non-sterilized and sterilized ME and the corresponding aqueous solution at a drug concentration of 0.1%w/v.

Table 3
DEXP permeation parameters of non-sterilized and sterilized DEXP-M9 ME formulae and the corresponding aqueous solution.

Permeation Parameters	Aqueous solution	Non-sterilized ME formula	Sterilized ME by aseptic filtration
Jss (μg/cm^2/h)	30.35 ± 1.40	120.51 ± 4.50	126.58 ± 4.25
P_{app} (cm/h)	0.033 ± 0.001	0.134 ± 0.005	0.141 ± 0.005
D (cm^2/s)	0.015 ± 0.001	0.250 ± 0.019	0.271 ± 0.013
ER	—	3.97 ± 0.14	4.17 ± 0.14

N.B.: Jss: Drug transcorneal flux at steady state; P_{app}: apparent permeability coefficient; D: diffusion coefficient (D), ER: Enhancement ratio compared to the reference aqueous solution.

Fig. 5 **(A)** and Fig. 5 **(B)**, respectively. By capturing CLSM z-stack images of the cornea, conjunctiva, and retina, we could notice that the labeled ME formula, M9, demonstrated deep penetration, reaching 7, 12 and 6 μm after 24 h, while after 72 h the detected fluorescence attained 24, 72 and 8 μm, respectively, as shown in Fig. 5**(C)**, Fig. S3, and Fig. S4, and Fig. 5**(D)**, Fig. S5, and Fig. S6. It is worthy to mention that no fluorescence was detected in the labeled solution after 72 h at different z-stacks in the cornea, conjunctiva, and retina. These findings confirm the strong penetration capability of the selected ME formula in reaching the deep structures of the eye compared to the DEXP solution. The presence of a large amount of SAAs, in addition to the small size of ME droplets, led to deeper penetration of the formula into the different ocular tissue layers compared to the labeled fluorescent dye solution (Üstündag-Okur et al., 2014).

3.9. Physical stability of the selected ME formula

Visual observation of the stored ME revealed that the formula remained clear and transparent with no evidence of precipitation for up to six months, which ensures good stability. The PS, PDI, ZP, and viscosity of the selected medicated formula and its corresponding plain formula were measured after storage at room temperature for six months, Fig. S7. It is obvious that the plain ME droplet size remained almost consistent during the whole storage period. The PS and PDI of the stored drug-loaded formula showed significant increases compared to those of the freshly prepared formula ($p < 0.05$), this could be due to the salted drug incorporation, which would increase the tendency of droplet aggregation (Bhardwaj et al., 1995). It is worthy to note that the droplet size of DEXP-M9 did not exceed 60 nm after a 6-month storage period. On the other hand, a non-significant increase in the ZP magnitudes and viscosity data was noticed ($p > 0.05$), which ensures high stability of both plain and drug-loaded formulae for a long period of time, up to six months, as previously described. To recapitulate, the drug-loaded w/o ME formula DEXP-M9 was chosen owing to its small droplet size (43 ± 5 nm), PDI (0.35 ± 0.07), adequate ZP (-12 ± 4 mV), and stability up to six months. The high permeation profile, powerful mucoadhesion, deep ocular penetration, and ease of sterilization make it an optimum candidate for further *in vivo* studies.

3.10. In vivo studies

3.10.1. Clinical inspection and scoring

The clinical signs of ocular inflammation in the right eyes are shown in Fig. 6. It can be observed that the negative control group (Group I) showed no signs of inflammation, congestion, or hyperemia of the iris with normal eye reflex and good eye condition during the whole experiment for 24 h with a score of 0 (Stonex et al., 2022). On the contrary, the LPS-induced eye uveitis (Group II, positive control) showed excessive signs of inflammation, which started immediately after LPS administration, increased progressively after 6 h, and worsened at 24 h, reaching a score of 4 (Stonex et al., 2022).

Group III treated with the drug solution revealed progressive eye inflammation, which reached its maximum after 12 h and continued in bad condition after 24 h with a score of 4. This can be attributed to the poor penetration of the hydrophilic DEXP salt through the lipoidal ocular mucosa, which results in a very poor anti-inflammatory effect. Noting that there was no significant difference between the DEXP solution and the positive control ($p > 0.05$) as observed in Fig. 6. Considering the selected ME formulations, the w/o ME (DEXP-M9) treated eye (Group IV) showed only mild irritation, which reached its maximum after 12 h but was resolved at 24 h and restored its normal condition with a very mild hyperemia (score of 1), comparable to the negative control group. The existence of large amounts of surface-active agents in ME enhances the permeation of the water-soluble DEXP, leading to its high penetration into the eye in sufficient amounts. In addition, the surfactants used (TPGS and Plantacare®) are biocompatible, which ensures the safety of the eye by inducing no ocular irritation. As a result, the anti-inflammatory effect of the drug was promoted, which eventually stimulated a calming effect in the eye and decreased the congestion. Moreover, the previously proven mucoadhesive effect

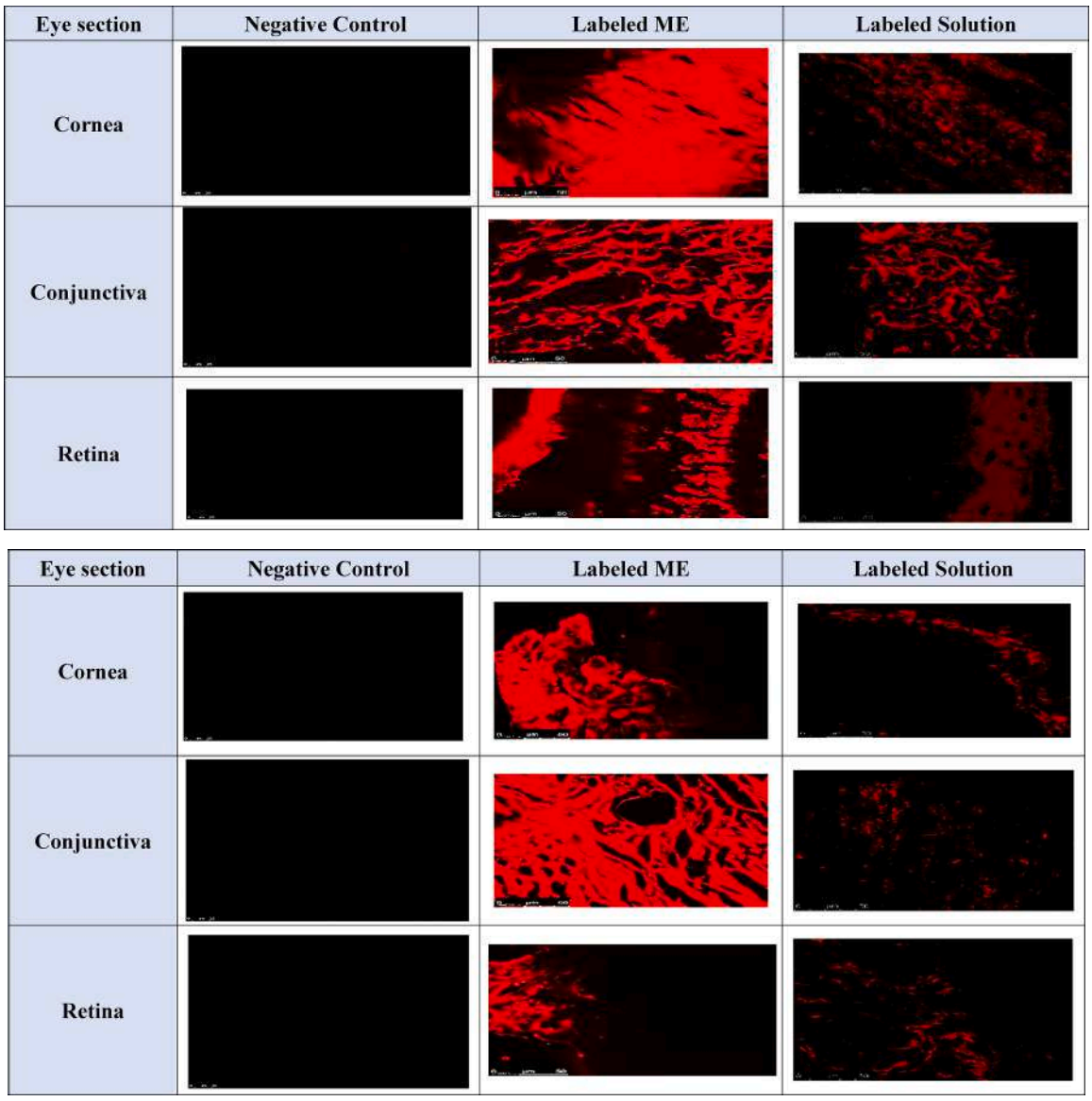

Fig. 5. Confocal images of different eye sections captured at the surface after instillation of Rhodamine-B labeled ME, M9, and solution compared to the negative control eye upon 24 h (A) and 72 h incubation (B), scale bar (50 μm). CLSM Z-stack scanning images of the cornea after 24 h (C) and 72 h incubation (D) with Rhodamine B labeled ME; M9, scale bar (50 μm).

increased the drug retention time and prevented drug loss through the nasolacrimal fluid, ending with a pronounced increase in drug bioavailability.

3.10.2. Histopathological examinations of the cornea, iris, and ciliary body

Considering the histopathological examination and evaluation of the three layers: cornea, iris, and ciliary body of different rat groups, the following was observed: the negative control (Group I) exhibited normal structure as the outer epithelium, inner endothelium, and intermediate stroma were intact, Fig. 7. The Bowman's membrane maintained a non-keratinized stratified squamous epithelium made up of continuous lamellae of uniform thickness. The keratocytes were flattened normal cells and dispersed between the stromal lamellae in the ground material. The cornea's inner endothelium was made up of a monolayer of flattened cells held together by a homogeneous Descemet's membrane. Similarly, the iris and ciliary body exhibited no signs of cellular infiltration, according to the findings (Ibrahim & Abd-Allah, 2022).

On the contrary, some epithelial cells were deformed, while others were degraded and vacuolated in the positive control (Group II). Other areas of the corneal epithelium showed localized disorder and stratification, while others showed focal irregularity and destruction. Furthermore, the corneal epithelium displayed vacuolated cytoplasm as well as some hyperchromatic, pyknotic cells. Stroma had an indefinite structure, with the collagen fibers destroyed and separated by large gaps with extensive cell infiltration in the iris and ciliary body.

For the drug solution group, Groups III, some epithelial cells with vacuolated cytoplasm were seen, and collagenous fibers were settled in the stroma with some intervals between them. Less cellular infiltration was noticed within the anterior segment of the iris compared to the positive group. While for the selected ME formulae (DEXP-M9), the corneal specimens indicated a nearly normal histological structure with intact epithelium, the Bowman's membrane appeared to be in a well-defined condition. The stroma contained flattened and ordered keratocytes. The membrane of Descemet and the endothelium appeared to be normal and continuous. The two treatment groups reduce the histopathological alterations caused by LPS extensively compared to the

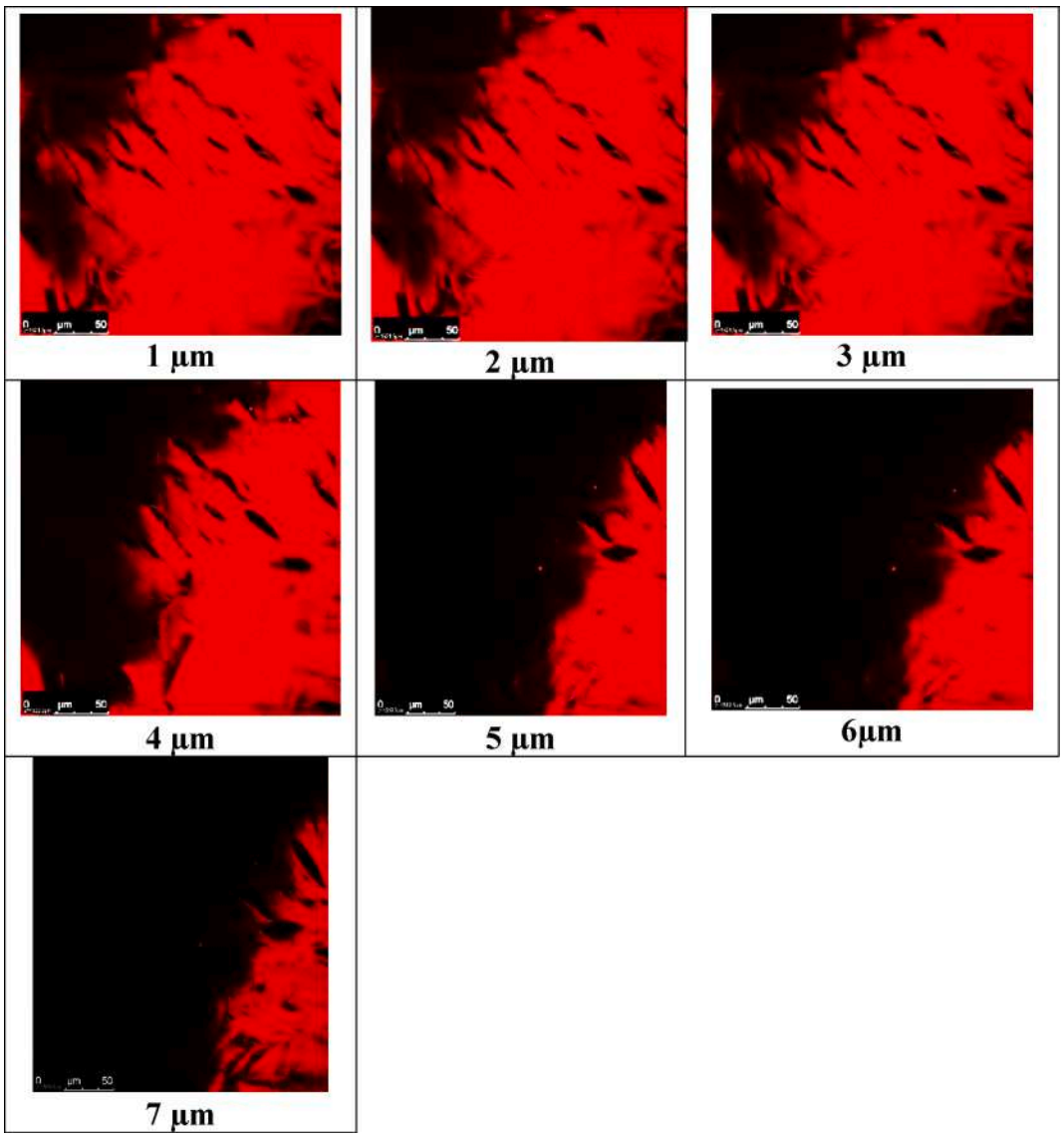

Fig. 5. (*continued*).

reference group, with a higher anti-inflammatory effect noted in the ME group. The poor penetration of the hydrophilic moieties across the eye mucosal layers could explain the lower clinical efficiency of the reference drug solution (Papangkorn et al., 2018).

3.10.3. Quantitative determination of TNF-α and IL-6 levels

The EIU is a model for animals used to access acute anterior eye inflammation. The most common characteristics of the EIU are infiltration of inflammatory mediators (neutrophils, monocytes, and dendritic cells) into the anterior of the eye segment and leakage of protein into the aqueous humor. The ultimate mechanism of EIU is not well understood. However, suggestions indicate that very high expression of cytokines, including the pro-inflammatory cytokines; TNF-α and IL-6, plays a magnificent role in the formation of EIU (Stonex et al., 2022).

The protein levels of TNF-α and IL-6 in the aqueous humor were evaluated using an enzyme-linked immunosorbent assay kit, as mentioned previously. The samples of aqueous humor from the eye of each animal were withdrawn and diluted with assay buffer. Equal amounts of aqueous humor were used for the measurement of TNF-α and IL-6. EIU is usually accompanied by the emergence of anti-inflammatory mediators, *viz.* IL-6 and TNF-α, where their estimation can be used as an indicator for the relief of eye inflammation (Otaka et al., 2023), where a significant decrease ($p < 0.05$) in the level of these mediators in the aqueous humor of the rats was recorded upon proper treatment with DEXP-M9.

Fig. 8 shows that the negative control (Group I) attained low amounts of TNF-α and IL-6 (94.4 ± 9 and 25.37 ± 1 ng/ml), respectively, which indicates a very low potential of irritation, while the inflamed eye of the positive control (Group II) suffered from a very high concentration of inflammatory mediators within the aqueous humor,157 ± 9.8 and 51.66 ± 1 ng/ml for TNF-α and IL-6, respectively, indicating severe irritation of the rat eyes, which are significantly different from the negative control ($p < 0.05$). The level of the inflammatory markers TNF-α and IL-6 in aqueous humor while using DEXP solution (Group III) showed very high levels (138 ± 13 and 59.3 ± 8 ng/ml) with no significant difference from the control without treatment, Group II ($p > 0.05$) owing to the very low permeation of the water-soluble drug across the lipophilic tissue of the eye, which ends in a very high irritation reaction of the drug solution.

However, the concentrations of the inflammatory mediators in aqueous humor while using w/o ME (DEXP-M9) in Group IV were reduced, reaching 93.53 ± 21.36 and 29.8 ± 5.4 ng/ml for TNF-α and IL-6, respectively, which differ significantly from the positive control ($p < 0.05$) with no significance from the negative control ($p > 0.05$) owing

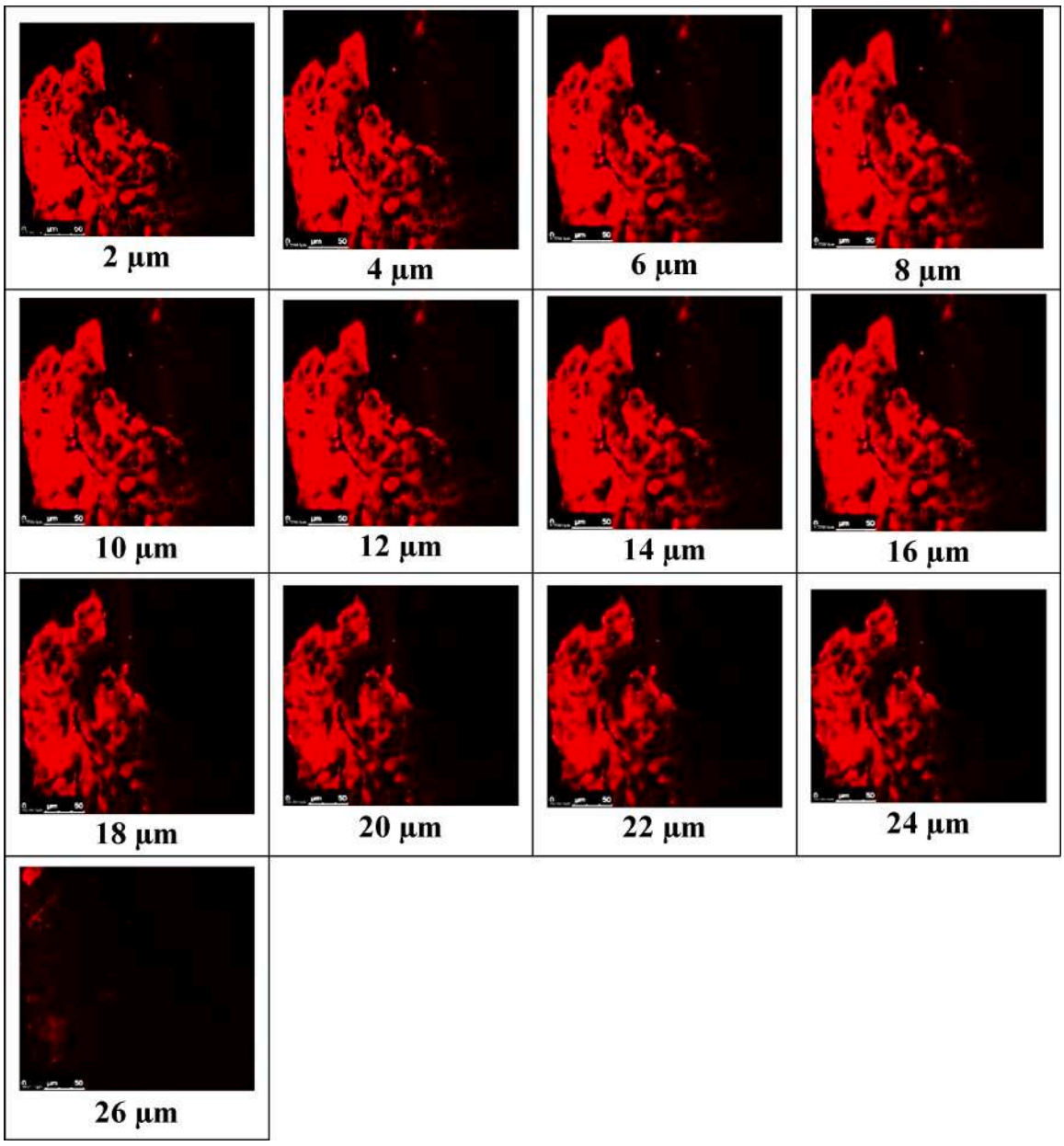

Fig. 5. (*continued*).

to the existence of large amounts of surfactants, which improve the permeation of the drug to the eye, and lead to minimal irritation compared to the drug solution. Moreover, there were significant differences between the ME formula, DEXP-M9, and the drug solution ($p < 0.05$), in favor of the ME formulae. From the previous results, it can be deduced that the selected ME formula DEXP-M9 succeeded in decreasing the inflammation more than the corresponding drug solution even at lower doses (1/4 dose of the reference product), which can lead to higher patient compliance and increased ocular safety due to a decrease in the total drug dose, which ends in lowering the systemic side effects (Gaballa et al., 2021; Ibrahim & Abd-Allah, 2022).

4. Conclusion

Successful biocompatible MEs were designed and prepared using Plantacare®818-UP and TPGS as a novel Smix and Capryol ™ PGMC as the oil phase in the presence of double-distilled water. Plantacare® 818-UP and a TPGS: Plantacare mass ratio of (2:1) provided the largest ME region and the most stable ME formulae. The DEXP-ME scored a small PS (43 ± 5 nm), PDI (0.35 ± 0.07), ZP (-12 ± 4 mV) and was stable up to six months. TEM images showed a small droplet size for both plain and drug-loaded formulae, < 100 nm. Both plain and DEXP-ME formulae exhibited prompt mucoadhesion properties and a three-fold higher permeation profile compared to the drug solution. CLSM confirmed that the labelled ME formula had deeper penetration into the cornea compared to the labelled fluorescent solution. Aseptic filtration was chosen as the method of choice for ME sterilization. The *In-vivo* studies using the EIU model proved better clinical and histopathological evaluation of the selected ME formula compared to the reference drug solution as well as significant lowering of the mediators of inflammation, TNF-α and IL-6. The ME formula DEXP-M9 succeeded in decreasing the drug dose and frequency of administration, which will lead to higher patient compliance as well as an increase in ocular safety.

Rat Group	Time (h)					Median Score
	0	2	6	12	24	
Group I (Negative control)		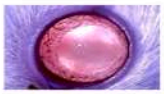	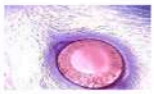			0
Group II (Positive control)						4
Group III (DEXP solution)	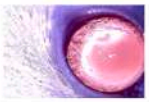	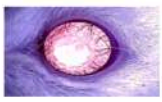		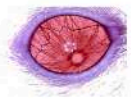		4
Group IV (DEXP-M9)	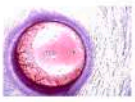				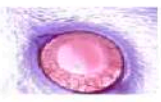	1

Fig. 6. Clinical evaluation and scoring of the rats' eyes of different treatment groups.

Rat Group	Cornea	Iris	Ciliary body	Median Score after 24 h
Group I (Negative control)	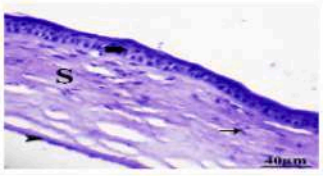		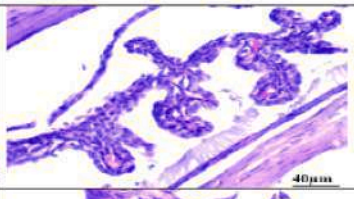	0
Group II (Positive control)	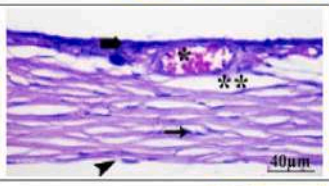	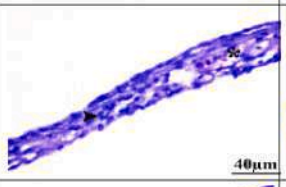	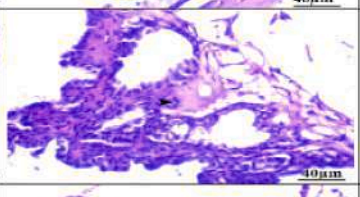	3
Group III (DEXP solution)	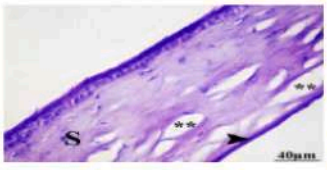	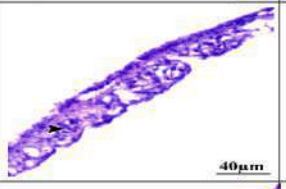	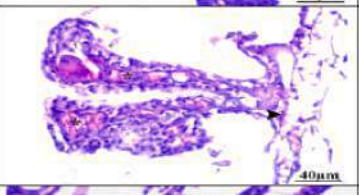	3
Group IV (DEXP-M9)	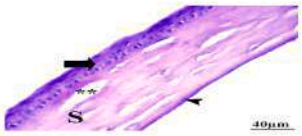	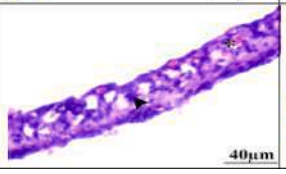	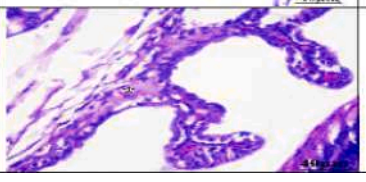	1

Fig. 7. Histopathological evaluation and scoring of the rats' eyes of different treatment groups showing outer epithelium (bold arrow), inner endothelium (arrowhead), intermediate stroma (S), and keratocyte (arrow).

Declaration of competing interest

The authors declare that they have no known competing financial interests or personal relationships that could have appeared to influence the work reported in this paper.

Data availability

No data was used for the research described in the article.

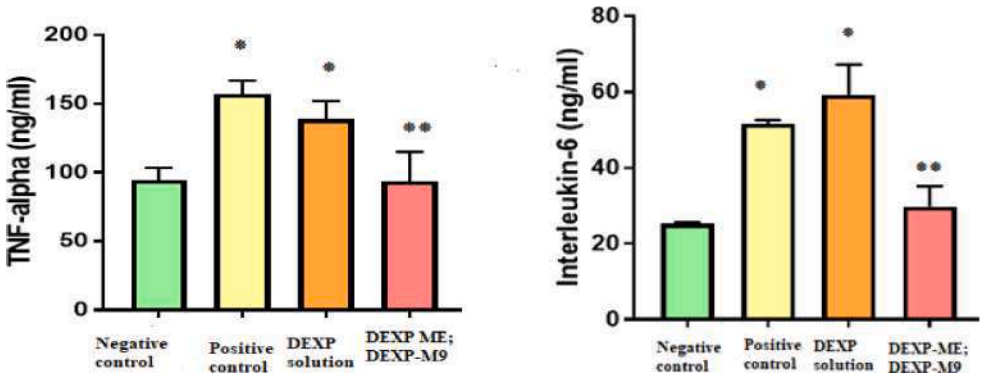

Fig. 8. Concentrations of (a) TNF-α and (b) IL-6 in aqueous humor samples of different rat groups 24 h-post treatment. *Significant difference *vs* negative control at $p < 0.05$, **Significant difference *vs* positive control at $p < 0.05$.

Appendix A. Supplementary material

Supplementary data to this article can be found online at https://doi.org/10.1016/j.ijpharm.2023.123704.

References

Abou-ElNour, M., Soliman, M.E., Skouras, A., Casettari, L., Geneidi, A.S., Ishak, R.A.H., 2020. Microparticles-in-thermoresponsive/bioadhesive hydrogels as a novel integrated platform for effective intra-articular delivery of triamcinolone acetonide. Mol. Pharm. 17 (6), 1963–1978.

Agarwal, P., Rupenthal, I.D., 2023. Non-aqueous formulations in topical ocular drug delivery–a paradigm shift? Adv. Drug Deliv. Rev. 198, 114867.

Ajaz, N., Khan, I.U., Khalid, I., Khan, R.U., Khan, H.A., Asghar, S., Khalid, S.H., Shahzad, Y., Yousaf, A.M., Hussain, T., Sabir, N., Ali, A., 2020. In vitro and toxicological assessment of dexamethasone sodium phosphate loaded pH sensitive Pectin-g-poly(AA)/PVP semi interpenetrating network. Mater. Today Commun. 25, 101325 https://doi.org/10.1016/j.mtcomm.2020.101325.

Akbari, E., Imani, R., Shokrollahi, P., Jarchizadeh, R., Heidari keshel, S., 2023. Hydrogel-based formulations for drug delivery to the anterior segment of the eye. J. Drug Delivery Sci. Technol. 81, 104250.

Al Saqr, A., Annaji, M., Poudel, I., Aldawsari, M. F., Alrbyawi, H., Mita, N., Dhanasekaran, M., Boddu, S. H. S., Neupane, R., & Tiwari, A. K. (2023). Topical Delivery of Diacetyl Boldine in a Microemulsion Formulation for Chemoprotection against Melanoma. *Pharmaceutics*, *15*(3), 901.

Ali, M.A., Rehman, N., Park, T.J., Basit, M.A., 2023. Antiviral role of nanomaterials: a material scientist's perspective. RSC Adv. 13 (1), 47–79.

Al-mahallawi, A.M., Ahmed, D., Hassan, M., El-Setouhy, D.A., 2021. Enhanced ocular delivery of clotrimazole via loading into mucoadhesive microemulsion system: In vitro characterization and in vivo assessment. J. Drug Delivery Sci. Technol. 64.

Bernal-Jácome, L. A., Izar-Landeta, J. M., Flores-Ramirez, R., i Farreras, J. M., & Vargas-Berrones, K. X. (2023). *Sustainable development and a performance assessment of Alkyl Polyglucoside as a substitute for Nonylphenol Ethoxylates in detergents*.

Bhardwaj, S.B., Shukla, A.J., Collins, C.C., 1995. Effect of varying drug loading on particle size distribution and drug release kinetics of verapamil hydrochloride microspheres prepared with cellulose esters. J. Microencapsul. 12 (1), 71–81.

Billowria, K., Sandhu, N.K., Singh, B., 2023. Topical Advances in Mucoadhesive Ocular Drug Delivery System. CDD 20 (8), 1127–1140.

Cardoso, C.O., Ferreira-Nunes, R., Cunha-Filho, M., Gratieri, T., Gelfuso, G.M., 2022. In situ gelling microemulsion for topical ocular delivery of moxifloxacin and betamethasone. J. Mol. Liq. 360.

Chambers, W.A., Green, S., Gupta, K.C., Hill, R.N., Huntley, K., Hurley, P.M., Lambert, L. A., Lee, C.C., Lee, J.K., Liu, P.T., Lowther, D.K., Roberts, C.D., Seabaugh, V.M., Springer, J.A., Wilcox, N.L., 1993. Scoring for eye irritation tests. Food Chem. Toxicol. 31 (2), 111–115. https://doi.org/10.1016/0278-6915(93)90123-G.

Cho, Y., Kim, S., Bae, E. K., Mok, C. K., & Park, J. (2008). Formulation of a cosurfactant-free O/W microemulsion using nonionic surfactant mixtures. *Journal of Food Science*, *73*(3), E115–E121.

Chu, K. O., Chan, K. P., Yip, Y. W. Y., Chu, W. K., Wang, C. C., Pang, C. P., 2022. Systemic and ocular anti-inflammatory mechanisms of green tea extract on endotoxin-induced ocular inflammation. *Frontiers in Endocrinology*, 1566.

Clausse, M., Payerlasse, J., Boned, C., Heil, J., Nicoles, L., & Zradba, A. (1983). *Solution properties of surfactants*.

Daston, G. P., & Freeberg, F. E. (2020). Ocular irritation testing. In *Dermal and Ocular Toxicology* (pp. 509–539). CRC Press.

De Caro, L., Del Giudice, A., Morin, M., Reinle-Schmitt, M., Grandeury, A., Gozzo, F., Giannini, C., 2023. Small Angle X-Ray Scattering Data Analysis and Theoretical Modelling for the Size and Shape Characterization of Drug Delivery Systems Based on Vitamin E TPGS Micelles. J. Pharm. Sci. 112 (1), 243–249.

de Oliveira Cardoso, V.M., Gremião, M.P.D., Cury, B.S.F., 2020. Mucin-polysaccharide interactions: A rheological approach to evaluate the effect of pH on the mucoadhesive properties. Int. J. Biol. Macromol. 149, 234–245. https://doi.org/10.1016/j.ijbiomac.2020.01.235.

Dutta, D., Setya, S., Gautam, N., & Talegaonkar, S. (2023). Encapsulation: Microemulsion. In *Principles of Biomaterials Encapsulation: Volume One* (pp. 157–195). Elsevier.

Eastoe, J., Hatzopoulos, M. H., & Tabor, R. (2013). *Microemulsions BT - Encyclopedia of Colloid and Interface Science* (T. Tadros (Ed.); pp. 688–729). Springer Berlin Heidelberg. 10.1007/978-3-642-20665-8_25.

Eastoe, J., Hetherington, K.J., Sharpe, D., Dong, J., Heenan, R.K., Steytler, D., 1997. Films of di-chained surfactants in microemulsions. Colloids Surf A Physicochem Eng Asp 128 (1–3), 209–215.

Elmotasem, H., Awad, G.E.A., 2020. A stepwise optimization strategy to formulate in situ gelling formulations comprising fluconazole-hydroxypropyl-beta-cyclodextrin complex loaded niosomal vesicles and Eudragit nanoparticles for enhanced antifungal activity and prolonged ocular delivery. Asian J. Pharm. Sci. 15 (5), 617–636.

Fujita, K., Kobayashi, M., Kawano, S., Yamanaka, M., Kawata, S., 2007. High-Resolution Confocal Microscopy by Saturated Excitation of Fluorescence. Phys. Rev. Lett. 99 (22), 228105 https://doi.org/10.1103/PhysRevLett.99.228105.

Gaballa, S.A., Kompella, U.B., Elgarhy, O., Alqahtani, A.M., Pierscionek, B., Alany, R.G., Abdelkader, H., 2021. Corticosteroids in ophthalmology: Drug delivery innovations, pharmacology, clinical applications, and future perspectives. Drug Deliv. Transl. Res. 11 (3), 866–893.

Gratieri, T., Gelfuso, G.M., de Freitas, O., Rocha, E.M., Lopez, R.F.V., 2011. Enhancing and sustaining the topical ocular delivery of fluconazole using chitosan solution and poloxamer/chitosan in situ forming gel. Eur. J. Pharm. Biopharm. 79 (2), 320–327.

Guo, Z., Guo, A., Guo, Q., Rui, M., Zhao, Y., Zhang, H., Zhu, S., 2017. Decomposition of dexamethasone by gamma irradiation: Kinetics, degradation mechanisms and impact on algae growth. Chem. Eng. J. 307, 722–728. https://doi.org/10.1016/J.CEJ.2016.08.138.

Hamed, R., Abu Kwiak, A.D., Al-Adhami, Y., Hammad, A.M., Obaidat, R., Abusara, O.H., Huwaij, R.A., 2022. Microemulsions as Lipid Nanosystems Loaded into Thermoresponsive In Situ Microgels for Local Ocular Delivery of Prednisolone. Pharmaceutics 14 (9), 1975.

Hanaa, M., Saleh, A.-S., Shaimaa, E., 2013. Design and optimization of self-nanoemulsifying drug delivery systems of simvastatin aiming dissolution enhancement. Afr. J. Pharm. Pharmacol 7 (22), 1482–1500.

Ibrahim, S.S., Abd-allah, H., 2022. Spanlastic nanovesicles for enhanced ocular delivery of vanillic acid: design, in vitro characterization, and in vivo anti-inflammatory evaluation. Int. J. Pharm. 625.

Jain, A., Khan, H. W., & Jain, P. (2023). Application of biosurfactant as versatile additives or ingredients of food processing. In *Applications of Next Generation Biosurfactants in the Food Sector* (pp. 111–135). Elsevier.

Kabalnov, A., Olsson, U., Wennerstroem, H., 1995. Salt effects on nonionic microemulsions are driven by adsorption/depletion at the surfactant monolayer. J. Phys. Chem. 99 (16), 6220–6230.

Kaur, A., Parmar, P. K., Jadhav, S., & Bansal, A. K. (2022). Advances in nanocrystals as drug delivery systems. In *Nanoparticle Therapeutics* (pp. 413–454). Elsevier.

Keck, C.M., Kovačević, A., Müller, R.H., Savić, S., Vuleta, G., Milić, J., 2014. Formulation of solid lipid nanoparticles (SLN): The value of different alkyl polyglucoside surfactants. Int. J. Pharm. 474 (1–2), 33–41. https://doi.org/10.1016/J.IJPHARM.2014.08.008.

Law, S.J., Britton, M.M., 2012. Sizing of reverse micelles in microemulsions using NMR measurements of diffusion. Langmuir 28 (32), 11699–11706.

Moghimipour, E., Salimi, A., Eftekhari, S., 2013. Design and characterization of microemulsion systems for naproxen. Advanced Pharmaceutical Bulletin 3 (1), 63.

Nguyen, H., Morgan, D.A.F., Forwood, M.R., 2007. Sterilization of allograft bone: is 25 kGy the gold standard for gamma irradiation? Cell Tissue Bank. 8 (2), 81–91.

Otaka, Y., Kanai, K., Okada, D., Nagai, N., Yamashita, Y., Ichikawa, Y., & Tajima, K. (2023). Effects of Oral 5-Aminolevulinic Acid on Lipopolysaccharide-Induced Ocular Inflammation in Rats. *Veterinary Sciences*, *10*(3), 207.

Palaria, B., Tiwari, V., Tiwari, A., Aslam, R., Kumar, A., Sahoo, B.M., Kumar, M., Singh, S., Kumar, S., 2023. Nanostructured Lipid Carriers: A Promising Carrier in Targeted Drug Delivery System. Current Nanomaterials 8 (1), 23–43.

Pantelic, I., & Cuckovic, B. (2014). Alkyl Polyglucosides: An emerging class of sugar surfactants. In *Alkyl polyglucosides* (pp. 1–19). Elsevier.

Papangkorn, K., Higuchi, J. W., Brar, B., & Higuchi, W. I. (2018). A novel ocular drug delivery system of dexamethasone sodium phosphate for noninfectious uveitis treatment. *Advances in the Diagnosis and Management of Uveitis*, 63.

Patel, H., Patel, J., Desai, B.G., Patel, K., 2010. Permeability studies of anti hypertensive drug amlodipine besilate for transdermal delivery. Asian J. Pharm. Clin. Res. 3, 31–34.

Rajput, A., Sharma, P., Sharma, R., & Thakur, S. (2022). *Novel Topical Drug Delivery Systems in Ophthalmic Applications*.

Ramos, M. F., Attar, M., Stern, M. E., Brassard, J. A., Kim, A. S., Matsumoto, S., & Vangyi, C. (2017). Safety evaluation of ocular drugs. In *A comprehensive guide to toxicology in nonclinical drug development* (pp. 757–811). Elsevier.

Rehman, M., Khan, M.Z., Tayyab, M., Madni, A., Khalid, Q., 2022. Self-Nanoemulsification of Healthy Oils to Enhance the Solubility of Lipophilic Drugs. JoVE 185.

Saadatmandi, A., Sohrabi, M.R., Kabiri Fard, H., 2023. Smart chemometrics spectrophotometry for rapid simultaneous quantitative determination of paracetamol, diphenhydramine, and phenylephrine in commercial tablet compared to high-performance liquid chromatography as a reference method. Chemom. Intel. Lab. Syst. 233.

Schmidt, T., Linders, J., Mayer, C., Cölfen, H., 2021. Determination of Particle Size, Core and Shell Size Distributions of Core-Shell Particles by Analytical Ultracentrifugation. Part. Part. Syst. Char. 38 (10), 2100079.

Shahab, M.S., Rizwanullah, M., Alshehri, S., Imam, S.S., 2020. Optimization to development of chitosan decorated polycaprolactone nanoparticles for improved ocular delivery of dorzolamide: In vitro, ex vivo and toxicity assessments. Int. J. Biol. Macromol. 163, 2392–2404.

Shakeel, F., Alamer, M.M., Alam, P., Alshetaili, A., Haq, N., Alanazi, F.K., Alshehri, S., Ghoneim, M.M., Alsarra, I.A., 2021. Hepatoprotective Effects of Bioflavonoid Luteolin Using Self-Nanoemulsifying Drug Delivery System. Molecules 26 (24), 7497.

Shi, X., Zhu, S., Jin, H., Fang, J., Xing, X., Wang, Y., Wang, H., Wang, C., Niu, T., Liu, K., 2021. The Anti-Inflammatory Effect of KS23, A Novel Peptide Derived From Globular Adiponectin, on Endotoxin-Induced Uveitis in Rats. Front. Pharmacol. 11, 585446.

Siafaka, P.I., Gündoğdu, E.A., Cağlar, E.S., Özgenç, E., Gonzalez-Alvarez, M., Gonzalez-Alvarez, I., Okur, N.Ü., 2023. Polymer Based Gels: Recent and Future Applications in Drug Delivery Field. *Current Drug Delivery*. CDD 20 (9), 1288–1313.

Singh, P., Chen, Y., Tyagi, D., Wu, L.i., Ren, X., Feng, J., Carrier, A., Luan, T., Tang, Y., Zhang, J., Zhang, X.u., 2021. β-Cyclodextrin-grafted hyaluronic acid as a supramolecular polysaccharide carrier for cell-targeted drug delivery. Int. J. Pharm. 602.

Stonex, T., Salmon, J.H., Adler, K.B., Gilger, B.C., 2022. Peptide Inhibitors of MARCKS Suppress Endotoxin Induced Uveitis in Rats. J. Ocul. Pharmacol. Ther. 38 (3), 223–231.

Suthar, T., Patel, P., Singh, P., Datusalia, A.K., Yadav, A.K., Jain, K., 2023. Hesperidin microemulsion: Formulation optimization, characterization, and in vitro evaluation. J. Drug Delivery Sci. Technol. 80, 104166.

Telò, I., Favero, E.D., Cantù, L., Frattini, N., Pescina, S., Padula, C., Santi, P., Sonvico, F., Nicoli, S., 2017. Gel-like TPGS-based microemulsions for imiquimod dermal delivery: role of mesostructure on the uptake and distribution into the skin. Mol. Pharm. 14 (10), 3281–3289.

Thummajitsakul, S., Piyaphan, P., Khamthong, S., Unkam, M., Silprasit, K., 2023. Comparison of FTIR fingerprint, phenolic content, antioxidant and anti-glucosidase activities among Phaseolus vulgaris L., Arachis hypogaea L. and Plukenetia volubilis L. Electron. J. Biotechnol. 61, 14–23.

Ugurl, T. (2023). *Managing allergic conjunctivitis via ophthalmic microemulsions: Formulation, characterization, in vitro irritation studies based on EpiOcular™ eye irritation assay and in vivo studies in rabbit eye*.

Ujhelyi, Z., Fenyvesi, F., Varadi, J., Fehér, P., Kiss, T., Veszelka, S., Deli, M., Vecsernyés, M., Bácskay, I.i., 2012. Evaluation of cytotoxicity of surfactants used in self-micro emulsifying drug delivery systems and their effects on paracellular transport in Caco-2 cell monolayer. Eur. J. Pharm. Sci. 47, 564–573. https://doi.org/10.1016/j.ejps.2012.07.005.

Üstündag-Okur, N., Gökçe, E.H., Eğrilmez, S., Özer, Ö., Ertan, G., 2014. Novel ofloxacin-loaded microemulsion formulations for ocular delivery. J. Ocul. Pharmacol. Ther. 30 (4), 319–332.

Wang, B., Zhu, Z., Yin, J., Lu, X., 2023. Microemulsion system formed with new piperazinium-based surface-active ionic liquid. J. Mol. Liq. 371.

Xiong, Y., Wang, T., Liu, L., Kou, Y., Zhao, Z., Yuan, M., Chen, Y., Wang, D., Song, S., 2023. Hydrogelation of TPGS for locoregional combination therapy of cancer. Chem. Eng. J. 451.

Yadav, U., & Ramana, K. V. (2019). Endotoxin-induced uveitis in rodents. In *Mouse Models of Innate Immunity* (pp. 161–168). Springer.

Yin, Q., Han, H., Shi, K., Zhou, J., Zheng, S., Yao, K., Shentu, X., 2023. Targeted dexamethasone nano-prodrug for corneal neovascularization management. Biomedical Journal.

Zaki Rizkalla, C.M., latif Aziz, R., Soliman, I.I., 2011. In vitro and in vivo evaluation of hydroxyzine hydrochloride microsponges for topical delivery. AAPS PharmSciTech 12 (3), 989–1001.

Zhang, M.i., Zhang, X., 2023. T cells in ocular autoimmune uveitis: Pathways and therapeutic approaches. Int. Immunopharmacol. 114.

Zheng, H. M., Li, H. Bin, Wang, D. W., & Liu, D. (2013). Preparation methods for monodispersed garlic oil microspheres in water using the microemulsion technique and their potential as antimicrobials. *Journal of Food Science*, *78*(8), N1301–N1306.

Zou, M., Jin, R., Hu, Y., Zhang, Y., Wang, H., Liu, G., Nie, Y., Wang, Y., 2019. A thermo-sensitive, injectable and biodegradable in situ hydrogel as a potential formulation for uveitis treatment. J. Mater. Chem. B 7 (28), 4402–4412.